Experimental characterization and numerical modeling of a viscoelastic expandable epoxy foam: Time–temperature transformation and time–temperature equivalence diagrams

Raffaele D'Elia, Leonardo Sanches, Jean Marie Des, Guilhem Michon

Experimental characterization and numerical modelling of a viscoelastic expandable epoxy foam: Time-Temperature-Transformation and Time-Temperature equivalence diagrams

Raffaele D'Elia [a,b,*], Leonardo Sanches [b], Jean Marie Des [a], Guilhem Michon [b]

[a] IRT Saint-Exupéry, 3 rue Tarfaya – CS34436 – 31405 Toulouse Cedex 4, France
[b] Université de Toulouse, ICA, CNRS, INSA/UPS/ISAE-SUPAERO/IMT MINES ALBI, Toulouse, France

Abstract

An expandable and Fire, Smoke and Toxicity (FST) compliant epoxy foam is proposed as an interesting alternative to Nomex® honeycomb cores for the development of Multi-Functional Structures (MFS). The paper first analyses the processing conditions using several experimental techniques as Differential Scanning Calorimetry (DSC), rheology and expansion in a closed volume in order to evaluate the reaction kinetics, the chemo-rheological behaviour and the expansion kinetics of the material. The experimental data are used to identify several empirical models describing the material processing behaviour and finally plotting the isothermal Time-Temperature-Transformation (TTT) diagram. A typical curing cycle for the foam is used to describe the evolution of the material parameters during the curing process. The fully-cured foam is then characterized using optical and laser microscopy in order to identify its cell size distribution and density. Quasi-static and dynamic machines are used to evaluate its mechanical and dynamical properties. The Time-Temperature equivalence is finally used to plot the master's curves of the material, representing the evolution of the material viscoelastic properties as a function of the frequency.

Keywords

Expandable foams, cure kinetic, multifunctional structure (MFS), Time-Temperature-Transformation diagrams, dynamic mechanical analysis, Time-Temperature equivalence

1. Introduction

Multifunctional structures (MFS) are composite materials typically used in aerospace applications, combining functional capabilities of one or more subsystems beyond the structural one, thereby reducing its overall mass and volume [1]. Among the different solutions available to develop MFS, the use of sandwich panel structures is gaining increasing attention, because of their lower areal density, durability and cost. Typical composite sandwich structures for aerospace MFS use Nomex honeycomb as core material, given their superior strength-to-weight-ratio and compliance with FAR and AITM FST regulations. However, their functionalization is quite difficult, given the complexity of their machining process. An effective solution to enhance the functionality of sandwich panel cores is the use of expandable polymeric foams, combining the ease of process with a favourable strength-to-weight ratio and excellent mechanical damping properties. The viscoelastic behaviour of the core material has a

* *Corresponding author*, raffaele.delia@mines-albi.f (R. D'Elia)

major impact on the final damping performances of the structure [2], [3]. Starting from this premise, new material concepts have been considered by customising their components, as syntactic foam composites with addition of nanoparticles [4]–[7], by using 3d printing technique for the structure realisation [8], [9], or considering multi-layered frequency-dependent material for damping improvements [3], [10]. An interesting example is the study conducted by Shahdin et al. [11], where the damping performance obtained with a Nomex-aramid honeycomb was compared with that obtained by using foam (Rohacell 51A) as core material. The comparison study reveals the damping performance is quite similar to each other up to the 3rd vibrating mode (around 2 kHz). Above this mode, the modal damping ratio observed with the foam becomes 25% bigger than the one with honeycomb configuration. Another study considered the application of absorbing foam as a passive damping medium to enhance resonance control of metallic thin-walled honeycomb structure [12].

Literature review is rich of works dealing with plastic foams processing and characterization: for thermoplastic polymers the most interesting works concern amorphous poly lactic acid (PLA), polyethylene (PE), polystyrene (PS) or polypropylene (PP) [13]–[16], while for thermoset most of the works deal with polyurethane (PU) foams, [17]–[19], because of their high versatility and wide range of applications. Great efforts have been performed as well for the modelling of the phenomena of nucleation and growth prediction within cellular plastic using different modelling theories [20]–[24] to predict the final cellular structure obtained depending on the processing conditions. Epoxy foams were first developed in the 1950s [25], [26] and adopted in the aviation industry during the 1970s [26], [27]. Despite being introduced in the aerospace industry for over half a century, their processing techniques and underlying mechanical properties remain to be fully comprehended. The processing of epoxy foams has been primarily studied experimentally and to a lesser extent compared to thermoplastic foams or polyurethanes. Most studies have centred on the mechanical properties of fully polymerized foam [28], [29] and on the foam-forming [30] [31]–[33].

Three main technologies are used to produce epoxy foams: epoxy resin mechanical mixture with hollow microspheres (Epoxy Syntactic Foams, ESF), physical or chemical foaming by addition of a Physical Blowing Agents (PBA) or Chemical Blowing Agent (CBA) [26], [34]. ESFs are produced by adding hollow microspheres to the epoxy resin prior to curing, resulting in properties that are highly dependent on the type of microspheres and their compatibility with the epoxy resin [34]. Physical foaming can be implemented either by adding a substance changing its state as water [25], [35], or a gas as Freon [36] or simply raising the temperature of the polymer until its boiling point, assuring a cure kinetics that would freeze the final cellular structure and avoid thermal degradation [37]. A typical CBA used to produce epoxy foams is H-terminated polysiloxane [31], [38], [39]. The molecule is added to the pure resin without any risk of starting the expansion reaction, which is initiated right after the mixing with the amine based curing agent, as presented in Figure 1. The foaming process is associated to the Reaction A, where hydrogen gas is generated by the hydro-siloxane moiety with the curing agent. The cure of the

system starts simultaneously with a slower reaction kinetics (Reaction B), from a typical addition reaction between the epoxy-amine groups. Alternative CBA for epoxy foaming are trimethoxy boroxine (TMB) [40], sodium borohydride (SBH) [41], nonane [33] or azodicarbonamide (ADCA) [42].

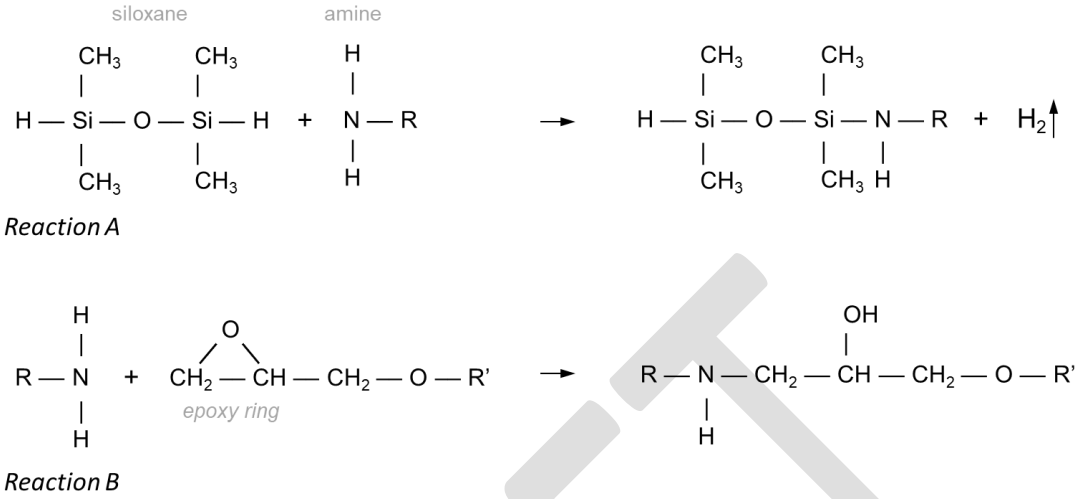

Figure. 1 Reactions of expansion between siloxane and amine curing agent (reaction A) with gaseous hydrogen release, and classical amine-epoxy groups addition reaction during epoxy curing (reaction B) [31].

Despite the widespread interest in using this material for aerospace applications, there is a lack of research in the literature linking the foaming reaction to its microstructure and final mechanical damping properties, resulting in a fragmented research landscape. Considering this, the aim of this paper is to characterize the reaction kinetics of an epoxy foam suitable for aerospace applications, modelling its physico-chemical behaviour in order to obtain a Time-Temperature-Transformation (TTT) diagram. The microstructure of the foam obtained using an optimized processing protocol will be characterized and finally the viscoelastic analysis of the material will be performed in order to establish a Time-Temperature equivalence to model the viscoelastic behaviour.

2. Material selection

The material selected for this study is an expandable and FST compliant epoxy foam supplied by Sicomin, the PB270i, with its curing agent SD 2630. The properties of the two products are summarized in Table 1, as proposed by the supplier in the Technical Datasheet (TDS) [43], [44].

Product	*T [°C]*	*PB 270 i*	*SD 2630*
Viscosity [mPas] Rheometer CP 50 mm, shear rate 10/s	20	22 000 ± 4 000	250 ± 50
	25	12 000 ± 2 500	150 ± 30
	30	7 500 ± 1 500	100 ± 20
	40	3 500 ± 700	50 ± 10
Density [g/cm^3] ISO 2811-1	20	1.23 ± 0.01	1.00 ± 0.01

Table 1 Properties of PB 270 i and SD 2630 according to the TDS from Sicomin.

The PB 270i has been chosen for its compliance with typical FST regulations as CS 25/FAR 25, assuring its potential use in aircraft in the cabin interior or MFS applications. The SD 2630 curing agent has been

chosen in particular for its very slow reaction kinetics in order to assure a complete polymerization and a theoretical higher glass transition temperature, according to the supplier. The mixing ratio initially proposed by Sicomin is 100:27. This value will be taken as a parameter in the frame of this paper and will not be analysed further. The mixing ratio proposed assure a final expansion ratio V_f/V_0 of 4.37, calculated as the ratio between the initial density (1.18 g/cm^3 from Table 1, using the mixture law) and the final density after expansion and curing of the system (0.27 g/cm^3).

The two components are mixed during 2 to 3 minutes in order to obtain a homogeneous mixture. Expansion starts immediately after addition of the amine curing agent and presents a very high kinetics in the first hour at 20°C, as it will be shown later in the frame of this paper, followed by a slow curing reaction. A typical curing cycle will be detailed and analysed in the next section, after having identified the TTT diagram of the system.

The nature of the CBA is not detailed in the Technical Data Sheet (TDS) of the product and it was not possible to confirm its exact composition in the frame of this work. However, given the immediate expansion reaction generated by the mixture of the amine curing agent to the resin, it is possible to deduce that the CBA is directly pre-mixed in the epoxy resin and its composition can be supposed close to the polysiloxane chemicals. In fact, as mentioned in the literature review (Figure 1), this family of CBA directly reacts with amine curing agent after their addition to the epoxy resin, generating two parallel reactions: the expansion with di-hydrogen generation and the more classical epoxy-amine addition.

In a very first phase, the system has been characterized using DSC (Differential Scanning Calorimetry) and TGA (Thermo-Gravimetric Analysis) dynamic scans under nitrogen flow, in order to evaluate the different physico-chemical properties as the glass transition temperatures (Tg) of the uncured (Tg_0) and fully cured (Tg_∞) system, the enthalpy of polymerization (ΔH_{tot}) and the mass loss during the expansion, curing and degradation reactions. First analyses have been performed using a heating rate of 5°C/min, because at higher values degradation reaction starts before polymerization is completed. In the next section, several scans using different heating rates will be used to average the enthalpy of reaction.

In the first DSC dynamic scan at 5°C/min presented in Figure 2, Tg_0 at -35.6°C is clearly visible, followed by the exothermic signal of the enthalpy of polymerization, with an onset at 64°C. This first sweep at 5°C is followed by a quench down to 20°C and by a second sweep at 10°C/min in order to evaluate the Tg_∞ of the system, which correspond in this case to 119.4°C, as showed in Figure 2.

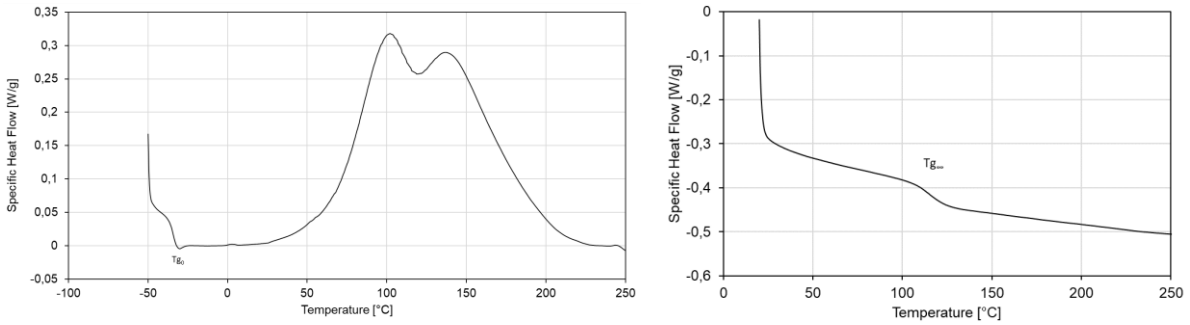

(a) (b)

Figure. 2 DSC dynamic scans performed on the system: (a) first sweep at 5°C/min and (b) second sweep at 10°C/min after complete cure of the system.

A TGA analysis of the system has been then performed at the same heating rate of 5°C/min on an uncured and fully cured system (Figure 3). The first curve (black, uncured sample) shows a mass loss of around 1.10% at 200°C, with a degradation onset at 307°C. The second curve on a fully cured sample presents a lower degradation onset at 290°C and a lower mass loss of 0.34% at 200°C, difference clearly arising from the expansion/curing reaction already completed for a fully cured sample.

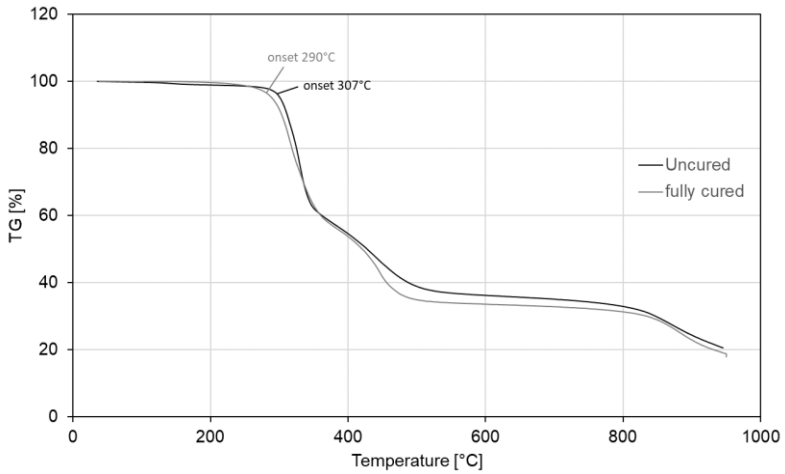

Figure 3. TGA curves performed on uncured and fully cured sample at 5°C/min under nitrogen.

The system has been particularly chosen for its compatibility with the FST requirements for aircraft interior cabin applications. The compliancy of the material with the FST standard CS25/FAR 25 25-853 for the 12 seconds flammability has been evaluated in August 2014 in DGA-CEAT, France (Report N°14-DGATA-MTF-P140003001004-F-A). These tests have been performed on the PB270i foam mixed with DM02 hardener, a different hardener from that used in this study and with a slower reactivity with regard to the SD2630. The data of the test have been supplied by Sicomin to the authors and show as the average burn length on three different samples is 7.6 cm (the limit of the standard is fixed at 20.3 cm for the 12 seconds flammability test).

3. Material processing analysis and modelling

3.1 Heat of polymerization and glass transition temperature

The total heat of polymerization (ΔH_{tot}) was measured using a series of dynamic scans from room temperature up to the completion of the cure of the sample using four different heating rates: 0.5°C/min, 1°C/min, 2°C/min and 5°C/min. These values were selected in order to avoid material degradation before the end of the exothermal peak of the reaction, phenomenon observed for heating rates higher than 10°C/min for the system under study. The results of these tests are presented in Figure 4.

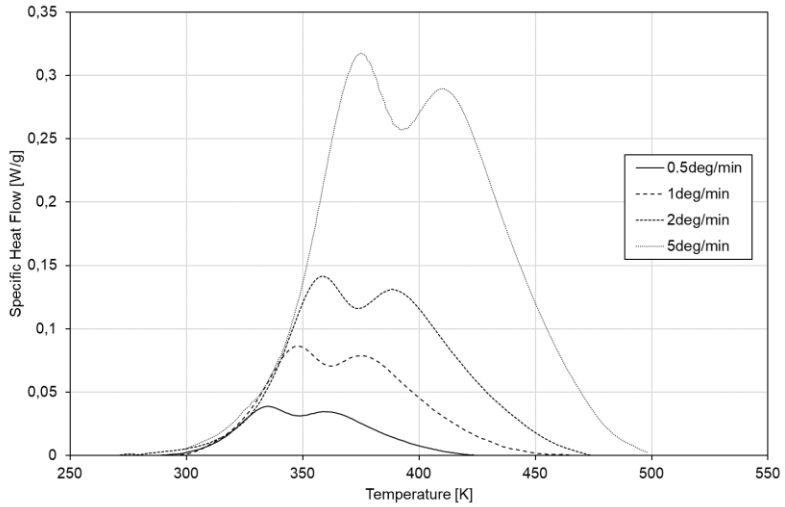

Figure 4. Specific Heat Flow of the PB270i/SD2630 system for different heating rates, from 0.5°C/min to 5°C/min.

The ΔH_{tot} represents the overall heat of reaction and is computed as the integral of the specific heat flow $\dot{H}$ over time using the following equation. The mean value obtained for this system is 322.4 (±21.1) J/g.

$$\Delta H_{tot} = \int_0^{t_f} \dot{H}\, dt \tag{1}$$

The glass transition temperature of the system (Tg) and the residual heat of reaction (ΔH_{res}) are determined after several idle times at several temperatures using DSC analysis. The degree of cure of the system is computed directly from the residual heat of reaction using the following equation:

$$\alpha = 1 - \frac{\Delta H_{res}}{\Delta H_{tot}} \tag{2}$$

Once both the degree of cure and the Tg are known for each experimental condition, it is possible to identify the Di Benedetto's formula for the system [45], as follow:

$$T_g = T_{g0} + \left(T_{g\infty} - T_{g0}\right) \cdot \frac{\alpha\lambda}{1-(1-\lambda)\alpha} \qquad \lambda = \frac{F_x}{F_m} \tag{3}$$

where T_{g0} and $T_{g\infty}$ are respectively the glass transition temperatures for uncross-linked (α = 0) and fully cross-linked polymer (α = 1), F_m and F_x are the segmental mobility of the corresponding physical states.

From the experimental DSC scans it is possible to identify the λ parameter of the system using a linearization of the equation (3) as follow:

$$T_g = A + B \cdot X \quad (4)$$

where A = T_{g0}, and B = $\left(T_{g\infty} - T_{g0}\right)$ and X = $\frac{\alpha\lambda}{1-(1-\lambda)\alpha}$. It is possible to make a correlation between this straight line and the experimental data obtained by DSC scans and determine the λ value assuring the best R^2 coefficient. In the present case a very good correlation between the experimental data and the model has been obtained (R^2 of 0.992) for a λ of 0.342. The other parameters obtained using the DSC analysis are summarized in Table 2, while the Di Benedetto's plot presenting the evolution of the Tg with the degree of cure is presented in Figure 5.

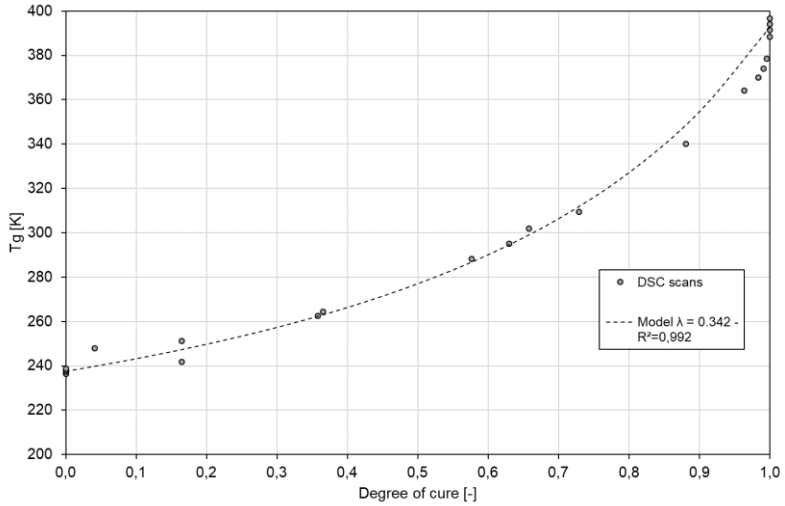

Figure 5. Di Benedetto's plot of the PB270i/SD2630 epoxy system.

Parameter	*Value*
ΔH_{tot}	322.4 (±21.1) J/g
T_{g0}	-35.6 (±1.0) °C (237.5 K)
$T_{g\infty}$	119.4 (±3.6) °C (392.4 K)
λ	0.342

Table 2 Overall heat of reaction and Di Benedetto's parameters.

3.2 Cure kinetics modelling

Cure kinetic modelling represents an essential step in the analysis of the processing of the epoxy foam: it allows estimating the evolution of the degree of cure of the system, and associate it with the different phenomena involved as gelation, vitrification, viscosity evolution and so on [46], [47]. In the literature two main identification methods of the reaction mechanisms of a chemical system are proposed: the isothermal analysis [48]–[54] and the isoconversional analysis [55]–[59]. Although the

isoconversional methods are very promising for the study of complex systems with several heterogeneous reactions involved, they are quite complex and very difficult to fit with isothermal data.

For this reason, the authors have used a more classical isothermal approach, composed of a series of isothermal DSC scans, where the temperatures are chosen in order to constitute a representative range for the reaction kinetics, previously analysed through different dynamic scans. A reaction model has to be chosen and numerically fitted with the isothermal DSC curves in order to obtain the kinetic constants and the reaction orders of the reaction. Among the wide variety of reaction models available in the literature [59], a typical phenomenological one used for epoxy systems has been proposed by Kamal and Sourour [60]. This model; composed of two kinetic constants (k_1 and k_2) and two reaction orders (n, m), represents quite well the autocatalytic and catalytic reaction mechanisms involved within the epoxy-amine chemical reaction. The equations of the model are the following:

$$\begin{aligned} \frac{d\alpha}{dt} &= (k_1 + k_2\alpha^m)(1-\alpha)^n \\ k_i(T) &= k_{0i} exp\left(\frac{-E_{0i}}{RT}\right)\ i = 1,2 \end{aligned} \tag{5}$$

This method generally neglects the thermal history during the heating rate that precedes the isothermal step of the analysis [53]. This initial ramp generates an initial degree of cure of the system α_0 that has to be considered especially for high temperature isotherms. The initial heating rate has two main effects influencing the initial degree of cure of the sample: first the advancement of the reaction, directly correlated to the thermal history of the sample before the isothermal step (direct effect); second an indirect effect upon the DSC curve itself, which does not allow to exploit the whole curve due to the C_p evolution during the dynamic scan. This second effect is more pronounced for higher temperature, where the initial degree of cure of the sample will be much higher. Besides all these aspects, this parameter α_0 can be easily obtained from two parameters: the isothermal DSC scan itself and the degree of cure at the end of the isotherm, obtained as previously explained from equation (2). The following equations hold:

$$\begin{aligned} \alpha_0 = \alpha(t_0) &= \alpha_f - \frac{\int_{t_0}^{t_f} \dot{H} dt}{H_{tot}} \\ \alpha_f = \alpha(t_f) &= 1 - \frac{\Delta H_{res}}{\Delta H_{tot}} \end{aligned} \tag{6}$$

where t_0 and t_f are respectively the starting and end times of the isothermal step. The introduction of the α_f parameter is necessary to consider the final degree of cure at the end of the isothermal step. When the isothermal step is long enough to complete the reaction, the α_f matches the maximum degree of cure at that specific isotherm (α_{max}). This third parameter is used to deal with the diffusion phenomena taking place when the glass transition temperature of the system attain the testing temperature [49], [50] and vitrification of the sample occurs. A first estimation of this parameter can be performed using the Di Benedetto's formula presented above in the text, although it is generally directly obtained from experimental DSC data [61]. In the present case the parameters α_f and α_{max} are considered as

equivalent and a trend for α_{max} is defined in order to take into account the diffusion-controlled zone. By considering these proposed modifications on the modified Kamal-Sourour model, the following relation is obtained:

$$\frac{d\alpha}{dt} = (k_1 + k_2\alpha^m)(\alpha_{max} - \alpha)^n \quad (7)$$

Once the model is fit with the different isothermal scans, it is possible to plot the natural logarithm of the two kinetic constants as a function of the reciprocal of the temperature (1/T). From this Arrhenius plot it is possible to identify the activation energy (the slope is $-E_a/R$, with R = 8.3144 $Jmol^{-1}$ K^{-1}) and the pre-exponential factor as the intercept of the line. The reaction orders *m* and *n* are averaged or eventually linearly fitted with a regression line, depending on their evolution with regard to the testing temperature.

In the present study the isothermal scans have been performed on a very wide range of temperatures, from 20°C (293.15 K) up to 150°C (423.15 K), in order to model the reaction kinetics on the whole range of processing temperatures of the epoxy foam. This wide range of temperature for kinetic modelling is not very common: indeed, reaction kinetic is generally identified on a very sharp window of temperatures, in order to represents exclusively the curing process. In the present study, the authors have decided to extend the temperatures for the identification of the kinetic of the system, in order to model the polymerization and expansion of the system. In fact, the foaming process takes places at room temperature (20°C), while the curing of the final product is performed between 40°C and 130°C, as previously explained in section 2. The kinetic parameters for the different isothermal scans are presented in Table 3. They are obtained from a direct fit with the experimental DSC curves using a *Nelder-Mead* simplex direct search algorithm [62], [63], through a *fminsearch* Scilab subroutine.

t_{cure} (h)	T_{cure} (°C)	k_1	k_2	*m*	*n*	α_0	α_{max}
48	20	2.61E-09	2.23E-05	0.12	0.89	0.01	0.66
12	40	4.95E-08	8.29E-05	0.13	1.03	0.03	0.73
8	60	7.45E-07	3.16E-04	0.13	1.15	0.23	0.88
8	80	8.71E-06	3.54E-04	0.11	1.23	0.14	0.96
5	120	8.38E-04	1.20E-03	0.09	1.48	0.42	0.98
5	150	4.50E-03	2.90E-03	0.11	1.70	0.73	1.00

Table 3 Kamal-Sourour parameters for isothermal modelling.

These data have been used to obtain the overall parameters of the model as explained above. The two rate constants k_1 and k_2 (Figure 6) are in very good agreement with the Arrhenius law, with correlation coefficients of respectively 0.998 and 0.973. Very good correlations have been obtained for the reaction orders as well (Figure 7). The first autocatalytic reaction order *n* follows a linear trend with the temperature, while the catalytic one *m* is almost constant over the whole temperature range. Concerning the α_{max} a good linear trend is observed for a temperature ranging from 20°C and 80°C (Figure 8), while for temperatures higher than 90°C, an extrapolation of the model will be considered and an α_{max} of 1 will be considered.

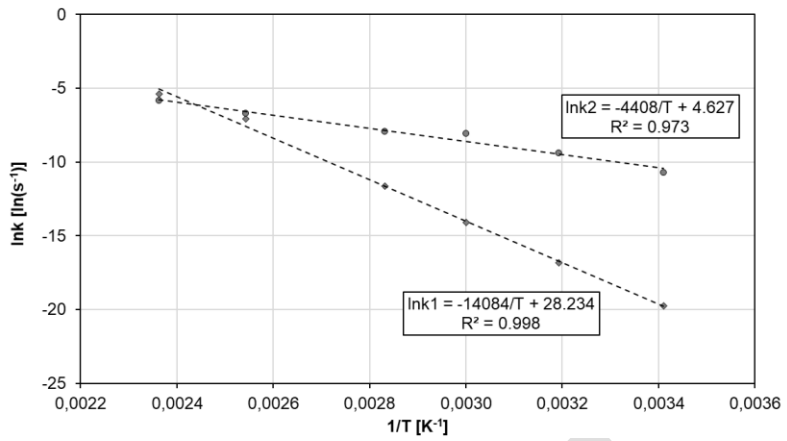

Figure 6 Arrhenius plot of the two rate constants of the system according to Kamal-Sourour model.

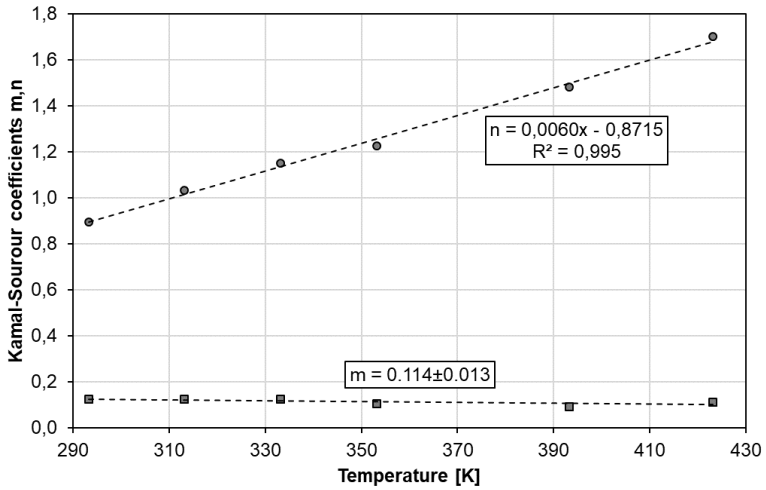

Figure 7 Reaction orders of the Kamal-Sourour model.

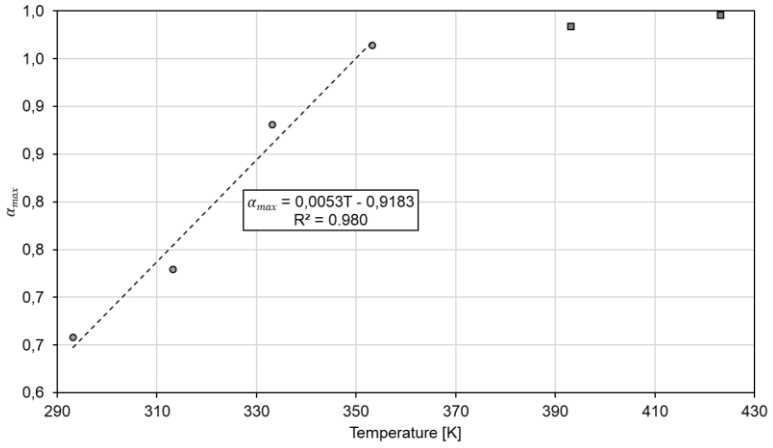

Figure 8 α_{max} evolution for the Kamal-Sourour model.

The final parameters of the Kamal-Sourour model obtained in agreement with these data are summarized in Table 4, while the degree of cure fitting with the DSC isothermal and dynamic scans are presented in Figures 9 and 10. The identified Kamal-Sourour model is globally representative of both

isothermal and dynamic conditions, with correlations factors R^2 ranging between 0.788 (iso60°C) and 0.999 (dynamic scan at 1°C/min). Concerning the isothermal conditions, it is possible to notice that the model is in good agreement with isothermal curves at 120°C and 150°C ($R^2 > 0.94$), while is partially satisfactory for the other isothermal curves at 20°C, 40°C, 60°C and 80°C (R^2 between 0.788 and 0.869). Dynamic scans are globally well represented by this model, although the reaction speeds for low reaction degree (< 0.6) are slightly different from the experimental DSC data. These different trends are globally dependent from the large spectrum of temperatures used and analysed. However, results are mostly reliable (R^2 >0.8), and can be considered as representative of the global trend of the material curing.

k_{01}=1.83E12 s^{-1}	k_{02}=1.02E02 s^{-1}
E_{01}=117.1 kJ/mol	E_{02}=36.7 kJ/mol
m = 0.114 ± 0.013	
n = 0.0060T - 0.8715	
α_{max} = 0.0052T – 0.8503	

Table 4 Kamal-Sourour parameters obtained with isothermal identification.

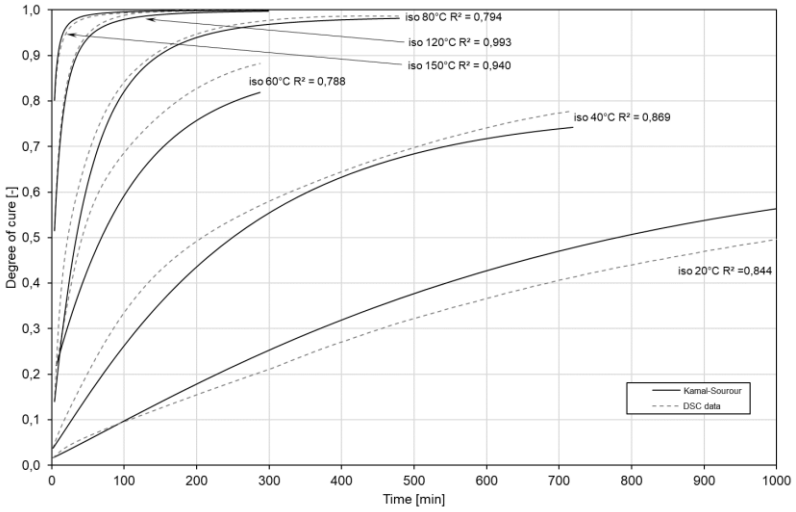

Figure 9 Degree of cure for different isothermal tests from 20°C to 150°C: DSC data vs. Kamal-Sourour model.

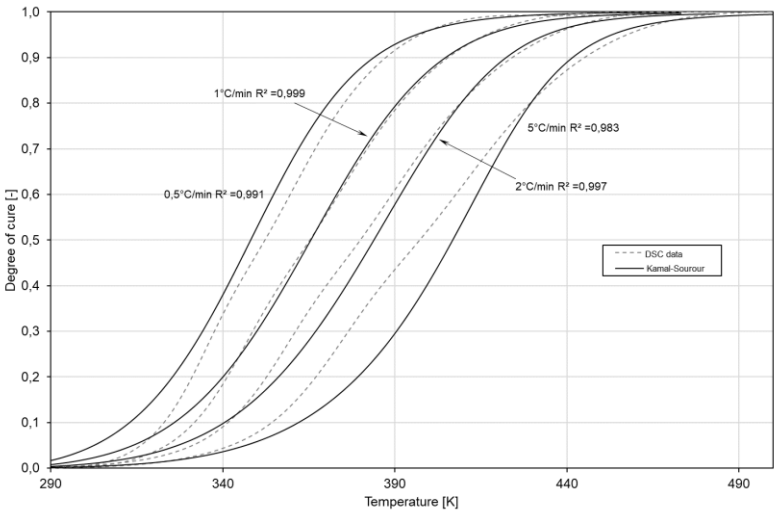

Figure 10 Degree of cure for different dynamic tests from 0.5°C/min to 5 °C/min: DSC data vs. Kamal-Sourour model.

3.3 Chemo-viscosity analysis: gelation and expansion

In order to analyse the viscoelastic behaviour of the foam during its processing, a series of dynamic and isothermal rheological tests have been performed under oscillatory conditions, with a frequency of 1 Hz and a strain amplitude of 1% in a plane-plane rheometer with an upper plate diameter of 20 mm. This analysis is commonly performed on thermoset polymers in order to follow the evolution of the complex viscosity ($\bar{\eta}$) and the complex shear modulus ($\bar{G}$) with temperature and time. According to the classical viscoelastic theory, if a sinusoidal strain $\varepsilon(t)$ with amplitude ε_0 and pulsation ω is applied to the polymer, the system will react with a sinusoidal stress $\tau(t)$, with an amplitude τ_0 and a pulsation ω, that will be shifted with regard to the strain of an angle δ, representing the loss angle. The complex shear modulus and viscosity will then be computed as follow:

$$\bar{G}(\omega) = \frac{\bar{\tau}(t)}{\bar{\varepsilon}(t)} = G'(\omega) + iG''(\omega) \tag{8}$$

$$\bar{\eta}(\omega) = \frac{\bar{G}(\omega)}{i\omega} \tag{9}$$

where the G' and G'' are respectively the storage and loss shear modulus of the system. The viscoelastic analysis of the system consists in the study of the evolution of these two parameters together with the tanδ as a function of time or temperature, for respectively isothermal or dynamic conditions. The goal of this analysis is the identification of the gel point of the system, corresponding to an irreversible phenomenon where the thermoset polymer transforms from a viscous liquid to an elastic gel. This point is defined as the moment when the average value of the molecular weight reaches infinity [46], [47], [64]. Once a thermoset has passed its gel point, it cannot be processed as a viscous liquid anymore and for this reason it is an essential parameter for the processing of a thermoset.

It is possible to correlate these parameters with the degree of cure using a kinetic model as the Kamal-Sourour that has been identified in this paper in the previous section. The goal of the viscoelastic analysis is to identify the gel point of the system under different conditions. Several criteria are proposed in the literature to evaluate the gel point for thermoset systems: the crossover of the G' and G'' curves [64][65], the maximum of the tanδ curve [66][67] or the point where the tanδ is independent from the frequency [68] are the most widely used, although the inflexion of G'' is a reliable method as well [53][66].

For a typical thermosetting polymer only one gel point is observed, since it depends only upon the cure kinetics and so on the densification of the molecular bridging of the system. In the present case, however, two phenomena have to be considered within the system: the foaming reaction, taking place in the very first phases of the cure, and the real gelation of the system taking place separately and farther in time if the expansion takes place at room temperature, as it is the case in our study. In analogy with the gelation criteria, it is possible to study the foaming process as well during the viscoelastic analysis, in order to identify a gel point of the foam during the expansion phase of the system. This approach has already

been successfully applied to the analysis of a polyurethane foam expansion within a plane-plane rheometer by Bouayard and co-workers [69]. According to their analysis and to several authors in the literature [70]–[75], the foaming process of a thermoset system can be divided into four steps: (i) induction time of degassing reaction, (ii) gas reaction, (iii) polymerization, (iv) consolidation. According to the experiment of Bouayard et al., a well-defined curve profile can be observed at the very beginning of the reaction, with the first three steps that can be clearly observed for a time lower than 150 seconds, while the so defined gel time of the foam, can be clearly identified as the cross-over of the two shear modulus.

In the present case, in order to obtain a homogeneous mixture of the two reactants of the system (expandable foam and hardener), the average preparation time of the sample before launching the rheometer tests ranged between 150 and 180 seconds. This preparation time seems to be too long in order to be able to observe the first three steps of the foaming process as described by the authors. For this reason, only the gel point of the system will be considered. In order to clearly separate it from the gel point coming from the curing of the system, this second gel point will be defined here as a *gel foam point* or simply *foam point*.

In order to analyse both the *foam gel point* (FGP) and the gel point (GP) of the system, first three dynamic tests in a rheometer have been performed using three different heating rates: 1°C/min, 2°C/min and 5°C/min. The two shear modulus G' and G'' and the tanδ are presented as a function of the degree of cure, computed according to the Kamal-Sourour model previously identified. Results are very close for the three tests and are presented here for the test performed at 2°C/min.

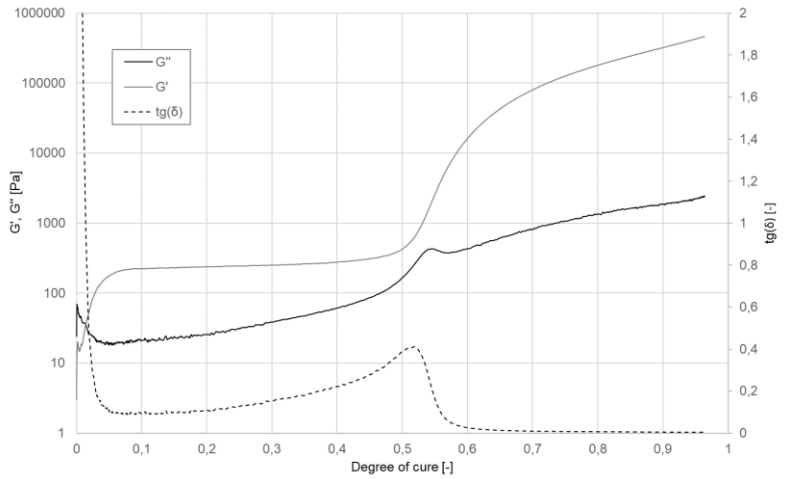

Figure 11 Dynamic scan at 2°C/min in a plane-plane rheometer on the expandable foam: $\boldsymbol{G'}$ and $\boldsymbol{G''}$ and the tanδ are presented as a function of the degree of conversion, calculated with the Kamal-Sourour kinetic model.

In all the curves it is possible to identify for a very low degree of conversion (0.014 – 0.016) the cross-over of the G' and G'' moduli, representing the *foam gel point*, while for a higher degree of conversion (0.519 to 0.585) the maximum of the tanδ criterion is clearly presenting the *curing gel point* of the sample. Results for the three heating rates are summarized in Table 5.

Heating rate (°C/min)	$\alpha_{foam\ gel}$	$T_{foam\ gel}$ *[°C]*	α_{gel}	T_{gel} *[°C]*
1	0.015	30.7	0.554	95.8
2	0.014	37.2	0.519	111.3
5	0.016	51.8	0.585	138.6

Table 5 Dynamic rheology tests: foam gel and curing gel points.

According to the dynamic tests, some temperatures have been selected to perform the isothermal scans under the same configurations (plane-plane oscillation, 1 Hz and 1% of amplitude). Two groups of tests have been performed in order to analyse the foam gel point (5 to 25°C) and gel point (100-120°C): results of these isothermal tests are presented in Figures 12 and 13 and summarized in Table 6.

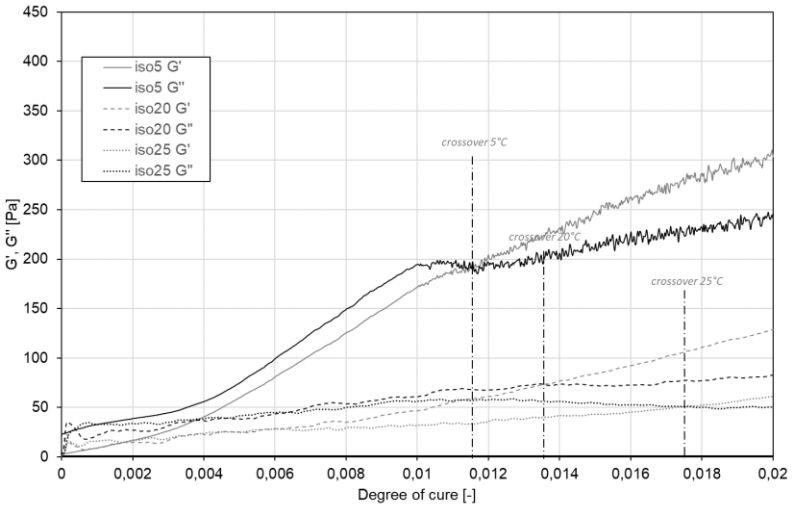

Figure 12 G' / G'' crossover for the three expansion tests performed within the rheometer at 5°C, 20°C and 25°C.

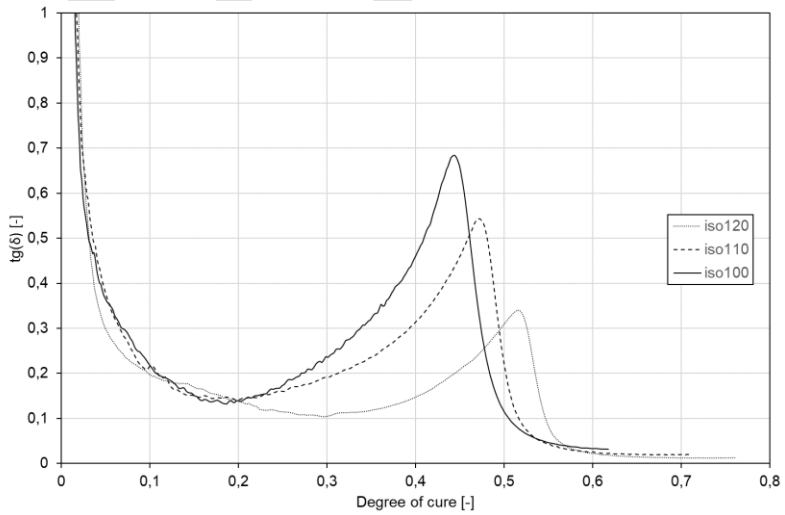

Figure 13 Tanδ evolution for isothermal tests at 100°C, 110°C and 120°C for the identification of the gel point of the system.

Figure 12 shows the crossover of G' and G'' as a function of the degree of cure computed with the Kamal-Sourour model. For a very low degree of cure ($\alpha < 0.02$) and temperatures ranging from 5 to 25°C, the crossover of the two moduli represents the *gel foam point*, representing the maximum densification of the bubbles within the foam. This analysis will be confirmed in the next session using

optical microscopy and a dedicated set-up developed to evaluate the expansion dynamic at room temperature.

In order to perform a gelation analysis at higher degree of cure and temperatures ($\alpha > 0.2$, temperatures ranging between 100°C and 120°C) a G'/G'' crossover criterion is generally used. However, in this particular case, the previously mentioned criterion cannot be directly applied due to the crossover occurring during the foaming phase, resulting in G'' constantly being lower than G'. This is a direct result of the porous structure that is created during bubble networking. To determine the gel point of the polymer, an alternative and effective criterion is often used in the literature based on the inflexion of the G'' modulus [53], [66]. Figure 11 demonstrates how the G'' inflexion corresponds to a clear maximum in the tanδ. This criterion has been ultimately utilized as the gelation criterion in Figure 13. Results of both analysis (foam gel point and gel point) are summarized in Table 6.

T [°C]	$\alpha_{foam\ gel}$	$t_{foam\ gel}$ *[min]*	α_{gel}	t_{gel} *[min]*
5	0.012	45.8		
20	0.014	22.7		
25	0.018	21.1		
100			0.494	24.6
110			0.559	22.5
120			0.644	21.5

Table 6 Isotherm rheology tests: foam gel and curing gel points.

Data obtained under both isothermal and dynamic conditions are very consistent and an average value has been computed for both foam gel and gel points, with an average error of respectively 13.9% and 9.4%:

$$\boldsymbol{\alpha_{foam\ gel} = 0.014 \pm 0.002}$$

$$\boldsymbol{\alpha_{gel} = 0.559 \pm 0.052}$$

3.4 Macroscopic expansion analysis

In order to confirm the expansion kinetics observed in the rheometer, a second experimental set-up has been used to evaluate the macroscopic behaviour of the foam during its expansion. To do so, the foam has been placed in a closed and known volume of air right after mixing. The volume of air is previously measured and the whole system is sealed and connected to a pressure sensor (*Inficom CDG*), capable of measuring very small variation of pressure. In accordance to the perfect gas law, in a closed volume and under isothermal quasi-static conditions, the following relation holds [76] :

$$p_0 V_0 = pV \tag{10}$$

where p and V stand for pressure and volume respectively. The index 0 stands for the initial conditions, while the values without index represent values as function of time. For instance, once the initial conditions (pressure and volume) are known, it is possible to compute in real time the exact volume from equation (10) simply reading the value of the chamber pressure as a function of time.

In order to be representative of a free expansion at constant pressure in air, the volume has to be very important in order to have a very limited pressure increase and a neglecting effect on the expansion dynamic. In order to identify the volume assuring these conditions, three different volumes have been tested using air balloons with different sizes, generating three different pressure increases on the foaming sample. All the experiments have been performed at 22 ± 1°C and 1008 ± 4 kPa of initial pressure. The results are summarized in the following table and presented in Figure 14.

Volume (cm^3)	*Pressure increase (kPa)*	*Expansion ratio at 120 min*
1395	2.16	2.35
3290	1.43	3.12
29780	0.19	3.59

Table 7: Results of the foam expansion in close volume.

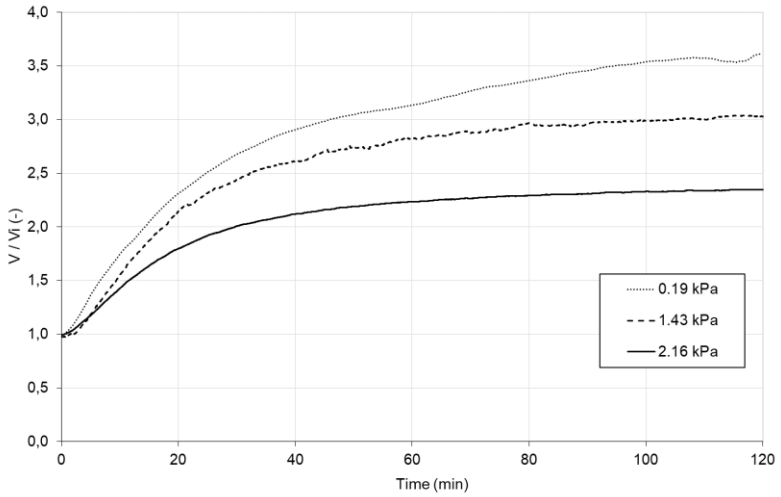

Figure 14: Expansion ratio vs. time for the three experiments performed.

It is interesting to notice that for a volume of around 30000 cm^3, the pressure increases of only 0.19 kPa. A further increase of the volume would generate an even smaller pressure increase, but it would be difficult to measure with the sensor used in the study. For this reason, this volume has been used for the following expansion analysis. The expansion curve obtained under these conditions can be fitted with an n^{th} order kinetic model [77], represented by the following equations:

$$\frac{d\beta}{dt} = k(1-\beta)^n \quad (11)$$

$$\beta = \frac{X-X_0}{X_f-X_0} \quad (12)$$

Where X represents the expansion ratio (V/V_0) at different instant during the test: X is the real time value, X_0 is the value at the beginning of the test and its equal to the unity, and X_f is the expansion ratio at the of the test. In this case, it has been supposed that the final expansion ratio is equal to the value obtained for a full expansion of the foam and a final density of 0.27 g/cc. This value has been measured on a fully cured foam, presented in the following, and are in agreement with that supplied by the foam

producer. This equivalent expansion ratio corresponding to the foam final density is of 4.37. The β value represents the degree of conversion of the expansion reaction: for $\beta = 0$ the expansion ratio is equal to unity (X_0=1), while for $\beta = 1$ the expansion ratio is equal to X_f = 4.37.

Under these conditions, the kinetic constant k of equation (11) has a value of 5.0E-4, while the reaction order n has a value of 2. The model and the experiment are both presented in Figure 15. An inflexion point of the curves at 22 minutes can be determined from the crossing of the two linear regions (t < 10 minutes and t > 40 minutes). Using the Kamal-Sourour model identified in section 3.2, it is possible to compute as well the degree of conversion (α) of the polymerization reaction, which is 0.016, in very good agreement with the $\alpha_{foam\ gel}$ value (0.014 ± 0.002) obtained from the chemo-viscosity analysis as the crossing point between G' and G". This result highlights a very interesting accordance between the two analysis (chemo-rheology and macroscopic expansion kinetic), confirming the good approach used in the study.

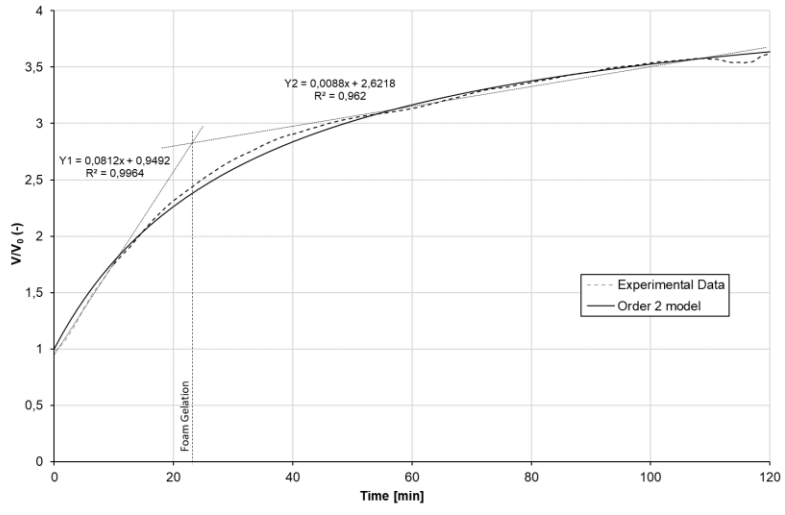

Figure 15: Foam expansion in a closed volume: experiment vs. modelling.

The process has been observed as well using a VHX7000 Keyence microscope with an objective VHX-E20 (x50 magnification), using a transmission light configuration. After a mixing time of 1'30", the foam has been placed on a standard microscope slide covered with a cover glass slip, in order to obtain a thin foam layer, enhancing the sharpness of the image and facilitate the identification of the bubbles. Images have been taken right after the mixing from 2 minutes to 90 minutes. The whole time-lapse is reported in Figure 16. Bubble nucleation takes place right after mixing, when the CBA reacts with the amine hardener. This phenomenon is clearly visible in the first image obtained 2 minutes after mixing. Bubble growth seems to be very fast before the foam gelation (t < 22'), strongly slowing down in the following (t > 22'), when bubble density has reached its maximum. In this first phase, bubbles coalescence does not seem to be a relevant phenomenon. However, for much longer times (30' < t < 90'), coalescence of the biggest bubbles is visible, when the bubbles clearly show a deviation from their initial circular form. These images confirm again that the maximum bubble growth is attained at the

foam gelation point (between 20 and 30' in this case), in agreement with both rheological and expansion tests.

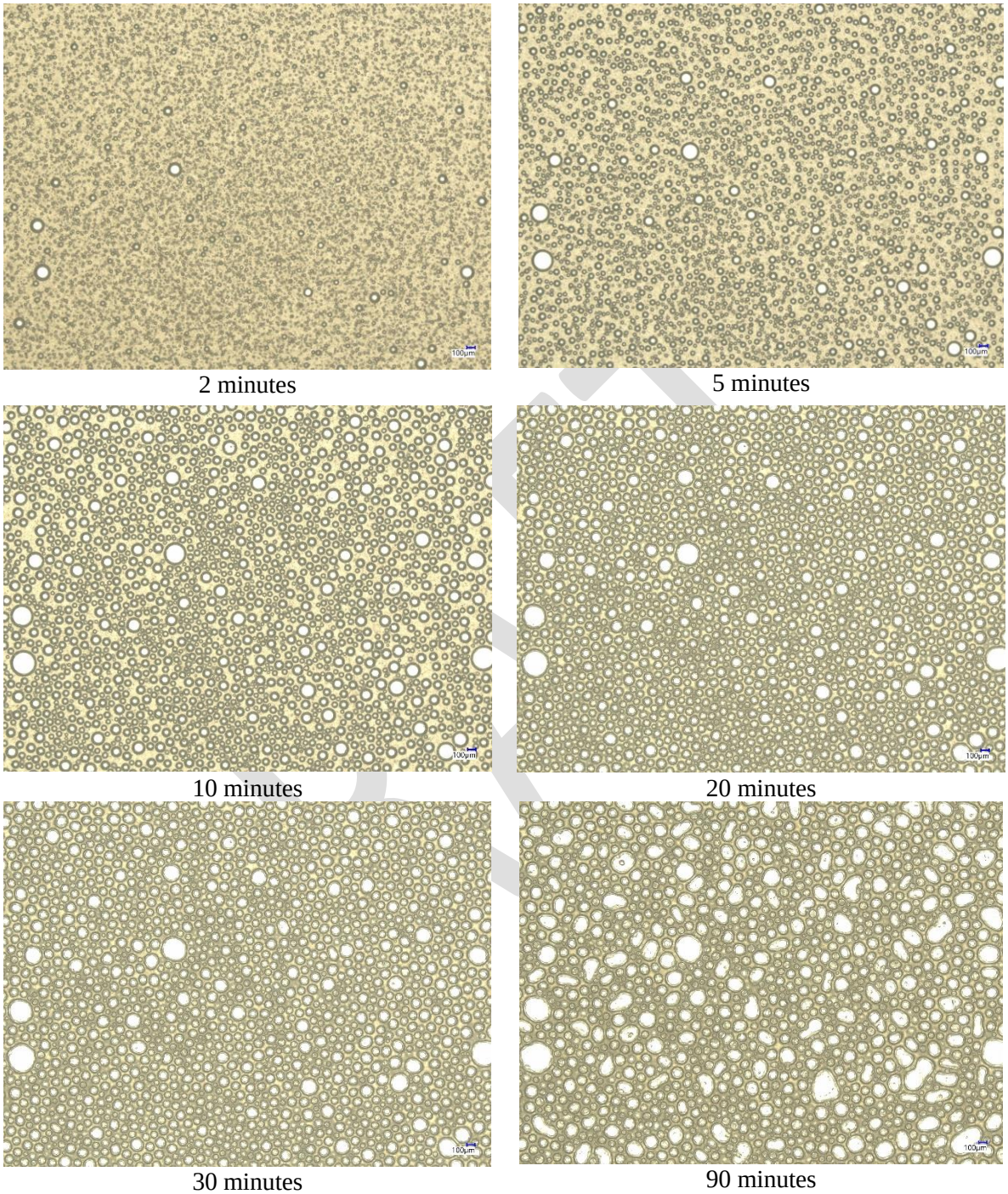

Figure 16: Foaming time-lapse using Keyence microscope.

3.5 TTT isothermal diagrams

Using the results obtained in the previous sections concerning the Di Benedetto equation for vitrification (Table 2), the Kamal-Sourour reaction kinetics model (Table 4) and the results of the chemo-viscosity analysis on the foam-gel and gel points (Table 6), it is possible to plot the TTT (Time-Temperature-Transformation) diagram of the system (Figure 17). The diagram presents the curves corresponding to

the different transformation taking place in this specific thermoset system, with on the Y axis the curing temperature and on the X axis the logarithm base 10 of the time. The t_0 of the diagram corresponds to the mixing time of the PB270i with its SD 2630 hardener. The four main curves presented are the foam-gelation curve, the gelation curve, the full curing curve and vitrification curve for this specific system. The curves corresponding to the different degrees of cure (10% to 90%) are presented in grey. According to the classical theory for TTT diagrams presented by Gillham [47], it is possible to define several physical states for the system considering Figure 17, described by several characteristic points summarized in Table 8.

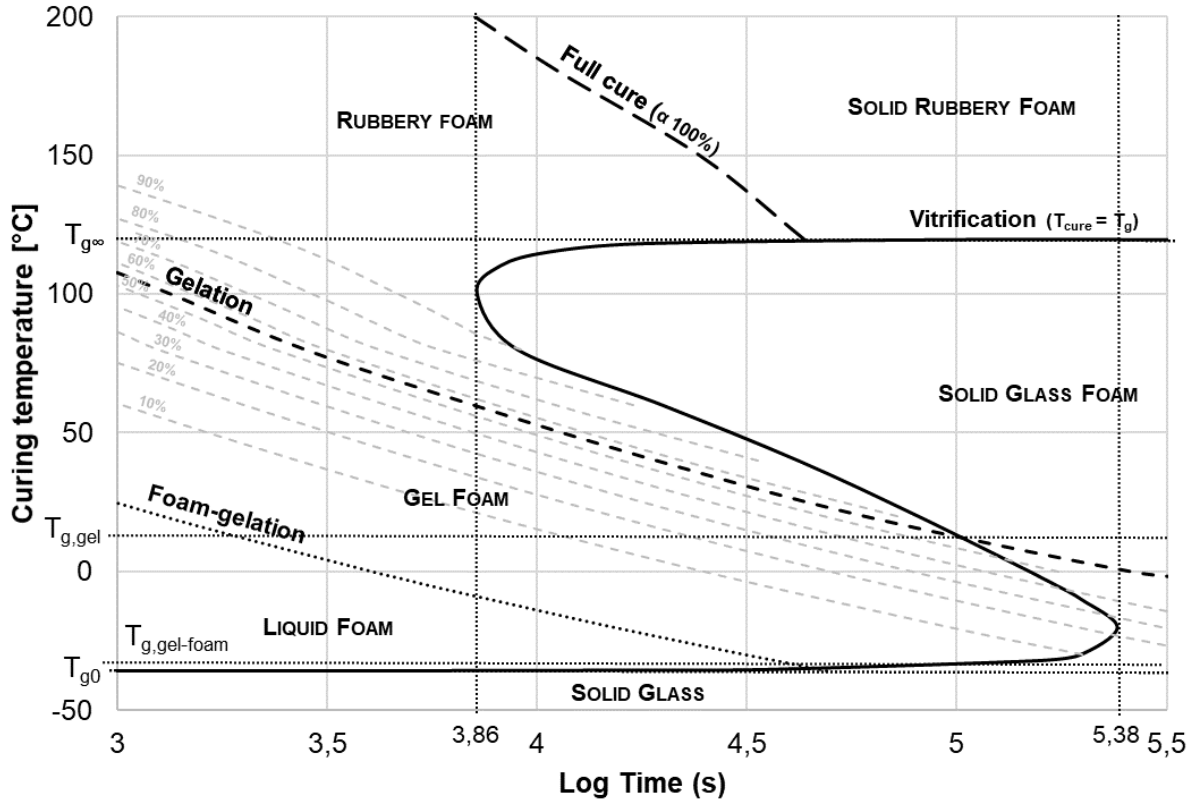

Figure 17: TTT diagram of the PB270i – SD2630 system.

Characteristic phenomenon	*Temperature (°C)*	*Time (hours)*
T_{g0}	-35.6	t_0
$T_{g,foam-gel}$	-34.9	11.1
Tangent 1	-20.0	66.6
$T_{g,gel}$	11.2	27.8
Tangent 2	100.0	2.0
$T_{g\infty}$	119.4	-

Table 8: Characteristic temperatures and times of the system.

The processing parameters obtained for the foam and used to plot the TTT diagrams presented in Figure 17 are summarized in the following table.

Processing modelling	
Cure kinetics (Kamal-Sourour model)	
k_{01}=1.83E12 s^{-1}	k_{02}=1.02E02 s^{-1}
E_{01}=117.1 kJ/mol	E_{02}=36.7 kJ/mol
m = 0.114 ± 0.013	
n = 0.0060T - 0.8715	
α_{max} = 0.0052T – 0.8503	
Expansion kinetics at 20°C (2nd order model)	
k=5.0E-4 s^{-1}	
n=2	
Gelification and expansion	
$\alpha_{foam\ gel}$ = *0.014 ± 0.002*	
α_{gel} = 0.559 ± 0.052	
Vitrification (Di Benedetto's equation)	
ΔH_{tot}: 322.4 (±21.1) J/g	
T_{g0}: -35.6 (±1.0) °C	
$T_{g\infty}$: 119.4 (±3.6)	
λ: 0.342	

Table 9: Characteristic temperatures and times of the system.

3.6 Curing cycle selection for bulk material characterization

Using the parameters identified in the previous section, it is possible to evaluate the theoretical evolution of the degree of reaction, glass transition temperature and expansion ratio during a typical curing cycle of the foam. The curing cycle selected for the following analysis of the cured foam, represents a compromise in order to obtain the highest expansion ratio at the end of the cure along with the highest Tg value, in agreement with the supplier recommendation. It is composed of several steps at different temperatures as follows:

24 h at 20°C, 24 h at 40°C, 2h at 60°C, 2h at 85°C, 2h at 110°C and 2h at 130°C.

In order to evaluate the parameters evolution during this specific cycle and compare their evolution with their prediction from the model, a foam specimen has been submitted to the complete cycle in an oven. At the end of each temperature step, a sample was extracted and characterized using DSC analysis: during a first sweep (5°C/min from -90°C to 250°C) the residual enthalpy of reaction and the glass transition temperature of the specimen are measured; during a second sweep (10°C/min from 20°C to 250°C) the eventual endothermal enthalpy of ageing and the Tg∞ of the system are measured. The results of the DSC analysis are presented in Figure 18 and their comparison with the kinetic modelling are summarized in Table 10.

The first step at 20°C is used mainly to reach the final degree of expansion proposed by the supplier. Using the expansion kinetics model, the degree of expansion at the end of this first step corresponds to 4.29, with a foam density of 0.275 g/cm^3, very close to the final value of 0.270 g/cm^3.

Considering the results obtained from the kinetic modelling for the curing process, they are globally in good agreement with the DSC experiments for the steps performed at 20°C, 40°C and 60°C. The modelling results are more diverging from the experiments performed on the last three steps at 85°C, 110°C and 130°C.

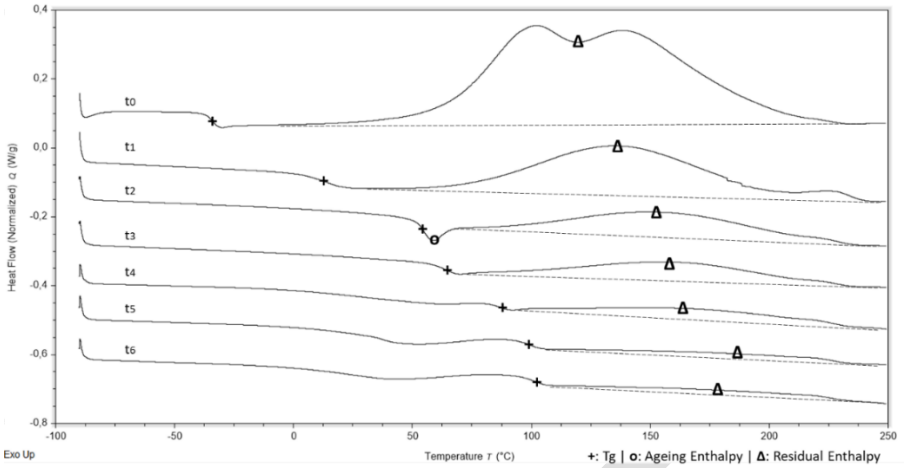

Figure 18: DSC scans at the beginning of the curing (t_0) and after the different curing step of the epoxy foam (t_1 to t_6).

Step name		t1	t2	t3	t4	t5	t6
Temperature (°C)		20	40	60	85	110	130
Duration (hours)		24	24	2	2	2	2
Degree of cure α	***Measured****	0.543	0.771	0.822	0.902	0.962	0.965
	Model	0.630	0.778	0.839	0.949	0.983	0.996
	Relative error	0.087	0.007	0.017	0.047	0.021	0.031
Tg (°C)	***Measured****	13.0	54.3	63.5	85.0	95.9	100.0
	Model	21.5	48.9	63.6	98.3	111.9	117.7
	Relative error	8.5	5.4	0.1	13.3	16.1	17.7
Residual Enthalpy of reaction (J/g)*		147.3	73.8	57.4	31.6	12.4	11.2
Ageing Enthalpy (J/g)		0.0	7.8	0.0	0.0	0.0	0.0
Tg∞ (°C)**		110.2	116.4	115.2	117.7	118.1	119.4

Table 10: Curing cycle: experiment vs. modelling (* 1st sweep at 5°C/min, ** 2nd sweep at 10°C/min).

This tendency can be mainly associated to the fact that a unique kinetic model has been chosen to describe the whole curing process from 20°C to 130°C. This choice creates an average representation of the different kinetics (expansion and curing) of the system and seems to affect much more the last steps of the curing process at higher temperature (T>85°C). In addition, the vitrification phenomenon has been described using a α_{max} linearly dependent from the temperature. This simplification seems to affect in particular the higher curing temperatures, where the Tg of the system is very close to the vitrification curve and so more affected by the diffusion-controlled kinetics. In addition, the Di Benedetto model presents a very important variation of the Tg with the degree of cure when the system approaches the $T_{g\infty}$. All these elements contribute on the final mismatch observed between the model and the experiments. The final degree of conversion measured for the system obtained using DSC scan is 0.965 (0.996 from the kinetic modelling), while the final Tg of the system is 100.0°C (117.7°C from the modelling). In order to improve the system kinetic modelling, a more accurate diffusion-controlled kinetics would be necessary instead of a simple α_{max} linear dependence from the temperature. This improvement would require more isothermal tests and won't be considered in the present study.

4. Material characterization after curing

4.1 Microstructure, density and static mechanical analysis

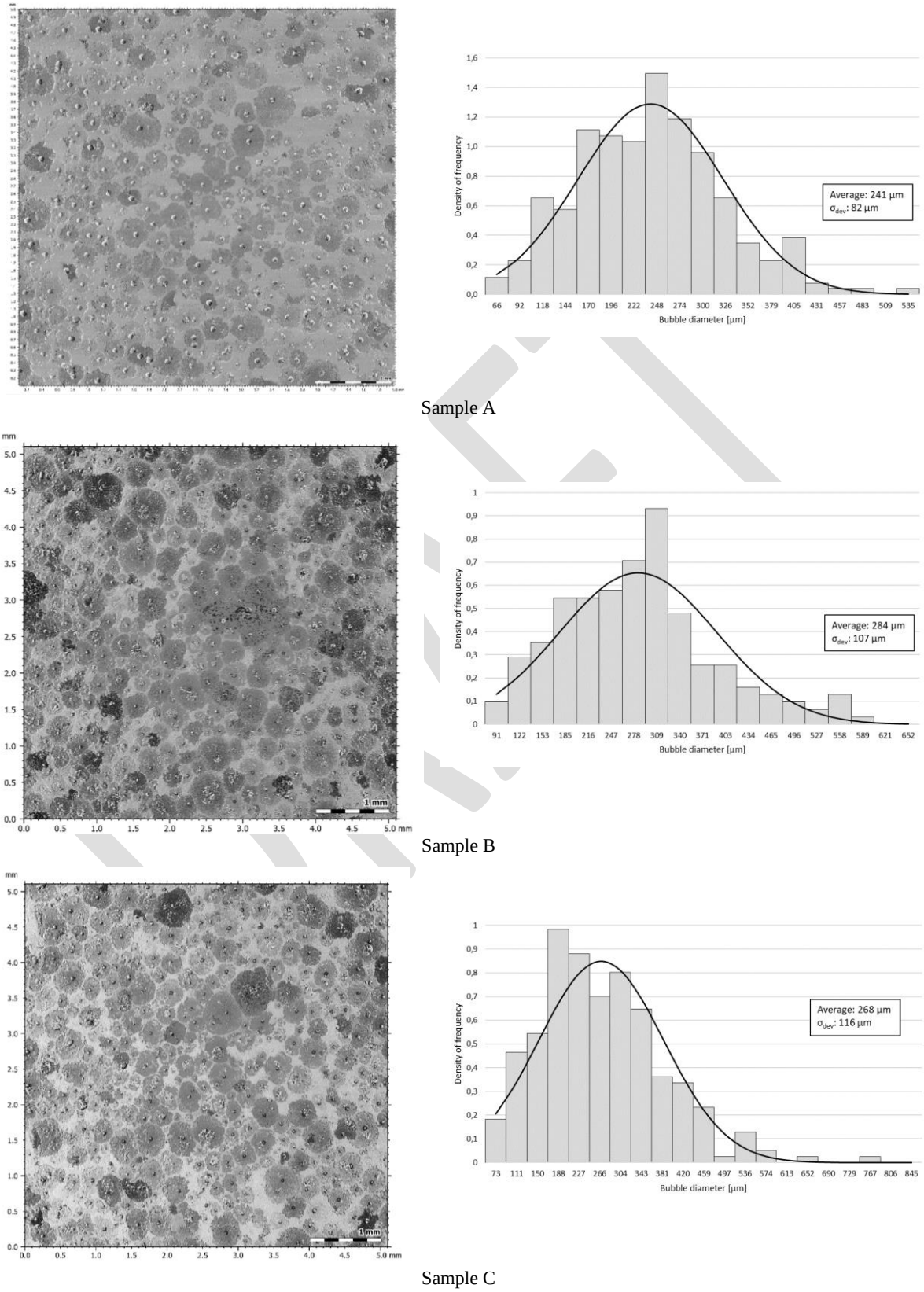

Figure 19: Microstructure of the bubbles obtained on three different samples cured with the cycle presented above.

In order to analyse the microstructure obtained with the selected curing cycle described in the previous section, several images have been taken and analysed using a laser confocal microscope (Zeiss LSM800) with a magnification of *2.5x* (*Numerical Aperture* 0.085, type *EC Plan Neofluar, Working Distance* 8.8 mm). The images are presented in Figure 19, with three different samples (A, B and C) cured with the same cycle presented in the previous section. Each micrograph (on the left of the image) is associated with its bubble statistical size analysis (on the right), with a normal distribution described by the average bubble size and its standard deviation.

In the three images, bubbles are clearly visible in dark grey, with the clearer zones representing the epoxy resin. At the centre of each bubble it is possible to notice a darker zone representing the original nucleus of the bubble, generated by the reaction of the CBA with the amine hardener. These nuclei present an average diameter of around 41 ± 7 µm. After nucleation, two main phenomena drive the expansion process, growth and coalescence of the bubbles, as largely described in the literature [22].

Using the open-source *ImageJ* software and its *ROI Manager tool*, images have been analysed and bubbles have been characterized by their equivalent diameter. The data have been collected and modelled using a classical normal Gauss distribution. The parameters obtained for the three images are summarized in the following table. An average bubble size of 264 ±102 µm is obtained.

Sample	***Average (µm)***	***σ_{dev} (µm)***	***Bubbles counted***
Sample A	241	82	267
Sample B	284	107	176
Sample C	268	116	247

Table 11: Results for the three samples analysed using the confocal microscope.

Apparent density of the samples has been measured as well, as the ratio between the mass and the apparent volume. For this purpose, ten different cubes have been developed and cured with the same curing cycle proposed above. A value of 0.272 ± 0.007 g/cm^3 has been obtained, in agreement with the supplier datasheet (final density 0.270 g/cm^3).

4.2 Material mechanical static and dynamic analysis

Considering the foam as an isotropic material, the static mechanical properties of the foam have been characterized through quasi-static tests on a standard hydraulic machine *Instron* equipped with a load cell of 10 kN. Two different tests have been carried out in order to identify the static Young and shear modulus E and G, respectively, and the Poisson ratio of the foam. For the Young modulus determination, cubes of around 20 mm x 20 mm x 20 mm have been submitted to compression loads with a displacement rate of 0.5 mm/min. An average value of 165 MPa for the Young modulus is determined through these tests.

Concerning the shear modulus evaluation, the material has been tested using a quad-shearing test with four samples assembled as presented in Figure 20. The material specimens consist in a parallelepiped

with transverse section of 100 mm² (10 mm x 10 mm) and length of 40 mm. The samples have been glued on the aluminium support using a classical *Loctite epoxy glue*. The average shear modulus obtained has a value of 61 GPa. Using the classical relationship between the Young modulus and the shear modulus, it is possible to finally compute the Poisson ratio of the material from the following equation.

$$\nu = \frac{E}{2G} - 1 \tag{13}$$

The value obtained for the Poisson's ratio of the foam is 0.35. The mechanical properties of the foam determined with quasi-static tests are summarized in Table 12.

Parameter	*Value*
E	165 MPa
G	61 MPa
ν	0.35

Table 12: Mechanical properties of the foam under quasi-static conditions.

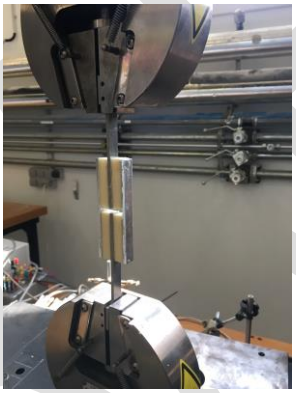

Figure 20: Quad-shearing test on the foam.

In order to evaluate the viscoelastic behaviour of the foam developed above, Dynamic Mechanical Analysis (DMA) under compression conditions have been carried out on a *Metravib DMA+1000* machine, using prismatic samples with a transversal section of 100 mm² (10 mm x 10 mm) and a length of 40 mm. Both form factor and stiffness of the samples are in agreement with the requirements specified by the machine's technical data sheet. This analysis is important in order to evaluate the viscoelastic intrinsic material properties of the foam, which are directly affected by the environmental and operational conditions and thus conditioning the structural response of the material during its life-cycle. For instance, in order to fully understand the material behaviour and evaluate a precise vibrational prediction of the industrial functionalized structures that would be developed with the PB270i foam, the evolution of the storage and dissipative modulus are investigated with regard to frequency and temperature domains.

A first iso-frequency analysis is performed in order to identify T_α of the material, representing the temperature at which the material loses its mechanical properties. The imposed mono-harmonic

deformation has the form of $\varepsilon = \varepsilon_m \cos(2\pi f t)$, with amplitude ε_m = 0.05 % and frequency f = 50 Hz, within a temperature range from 110°C to 180°C and a heating temperature rate of 2°C/min. The dynamic stress $\sigma(t)$ is computed through the measured dynamic force ($\sigma(t) = F/S$, F being the measured dynamic force and S the cross-section area of the specimen). The storage module ($E' = \frac{\sigma(t)}{\varepsilon(t)} cos\delta$), the loss modulus ($E''(t) = \frac{\sigma(t)}{\varepsilon(t)} sin\delta$) and the loss factor ($tan\delta = E''/E'$) can then be computed. E' and $tan\delta$ are presented in Figure 21. The T_α of the material obtained under these conditions has a value of 147 °C if the peak of the loss factor (tanδ) is considered. A loss factor of around 0.9 and a decrease of the storage modulus from 100 to 1 MPa is observed as well during the thermal transition. It is interesting to notice that this parameter T_α is quite different from the T_g measured using DSC analysis, which corresponds mainly to a C_p (Specific Heat) changing within the material more than a real mechanical property. Indeed, T_α is more than 30°C higher than the $T_{g\infty}$, which according to the DSC analysis represents the highest glass transition temperature attainable for this material. The difference observed between the two techniques is rather usual [78] and arises directly from the different principles and sensitivities of the two equipments used, along with the different masses, sample geometries, heating rates and frequency involved.

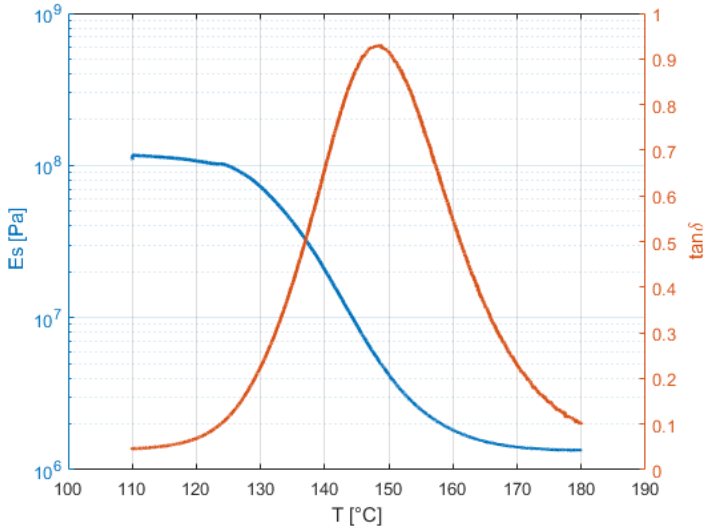

Figure 21: – Storage Modulus and loss factor of the epoxy foam PB 207i with respect to temperature variations

4.3 Time-Temperature equivalence and Master curves identification

In order to comprehend the evolution of the intrinsic material properties with respect to temperature and frequency variations, the Time-Temperature equivalence of viscoelastic materials is used to address the master curves of this foam. These curves are a useful tool to describe the evolution of the viscoelastic material properties for different range of frequencies (or times) and thus model its response under solicitations of different nature, frequency and intensity. The principle, first described by Leaderman in 1941 [79], describes how a viscoelastic material presents a similar behaviour if tested at high temperature and frequencies or at low temperatures and frequencies. The principle is described by the definition of master curves expressing dynamic variables E′, E′′ and tan(δ) in the frequency domain. The variables

are identified for a limited frequency range and for different temperatures. For this purpose, the simple thermo-rheological characteristic of the material has to be verified first using two different diagrams: the Cole-Cole diagram [80] and the Wicket diagram [81], illustrated in Figure 22 a and b, respectively. The first shows the relation between the loss modulus E" and the storage modulus E', while the latter shows the evolution of the loss angle δ with respect to the norm of the complex elastic modulus |E*|. As for the rheological analysis previously presented, the loss and storage modulus used in the DMA analysis are linked with the complex elastic module as follows:

$$\bar{E}(\omega) = E'(\omega) + iE''(\omega) \tag{14}$$

where ω represents the testing frequency. The above-mentioned diagrams are obtained through isothermal DMA analyses for a frequency range defined between 10 Hz and 100 Hz with 10 equally spaced points on a logarithm scale. The temperature range considered is defined within the interval of 125°C and 180°C. The continuity assured on the curves all along the different temperatures guarantees the simple thermo-rheological characteristic of the foam over the frequency and temperatures range studied.

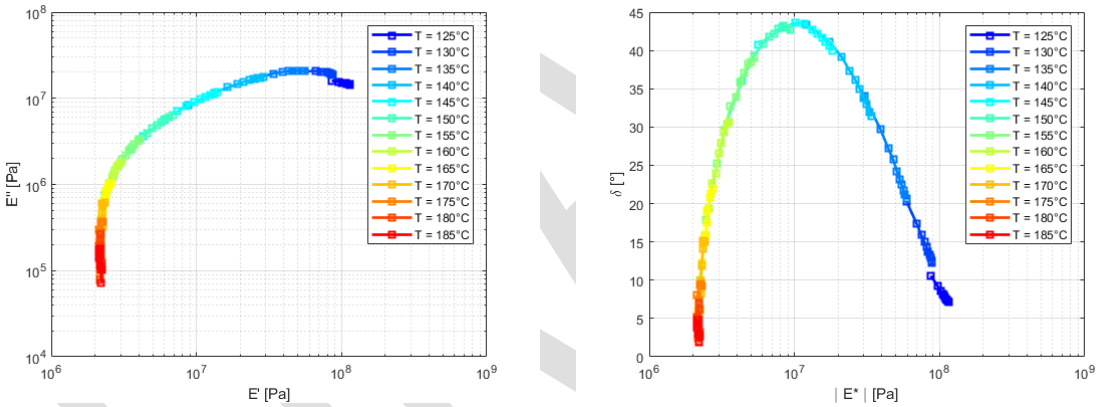

(a) (b)

Figure 22– Cole-Cole (a) and Wicket (b) diagrams of Epoxy Foam PB 270i.

The validation of the simple thermo-rheological characteristic done, it is possible to apply the Time-Temperature equivalence to the material. To do so, a displacement factor α_T associated to the horizontal translation of the curves E', E'' and tan(δ) versus frequency of each isothermal test is computed using DYNATEST® software. A reference temperature has to be used for the translation and in the present case a value of 145°C has been chosen. The evolution of the α_T as a function of the temperature as directly obtained from the software is presented in Figure 23 a. In order to use this parameter to plot the master's curves, the parameter has been fit using a Williams-Landel-Ferry (WLF) model according to the following equation [82]:

$$\log(\alpha_T) = \frac{-C_1^{ref}(T-T_{ref})}{C_2^{ref}+(T-T_{ref})} \tag{15}$$

The parameters obtained from the WLF model fitting with the displacement factor values are presented in the following table and allow plotting the curve presented in Figure 23 b.

Parameter	*Value*
T_{ref}	145°C
C_1^{ref}	4.811
C_2^{ref}	44.639 K

Table 13: WLF model parameters for the displacement factor.

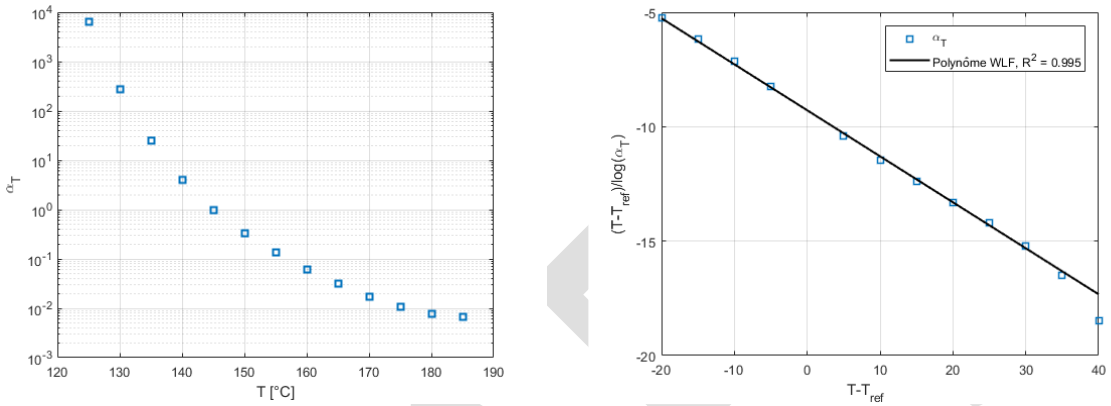

(a) (b)

Figure 23 – Isothermal displacement factor for a reference temperature of 145°C

Using the displacement factor obtained in Figure 23 a, it is possible to plot as well the three different master's curves of the material, presenting the dynamic material parameters as a function of the displacement factor. The curves are presented in Figure 24. The master curves presented in the figures are useful to predict the evolution of the mechanical properties of the material for a wide range of frequency at different operational temperatures. This procedure is highly envisaged in order to predict the vibrational response of functionalized industrial structures composed with the studied epoxy foam.

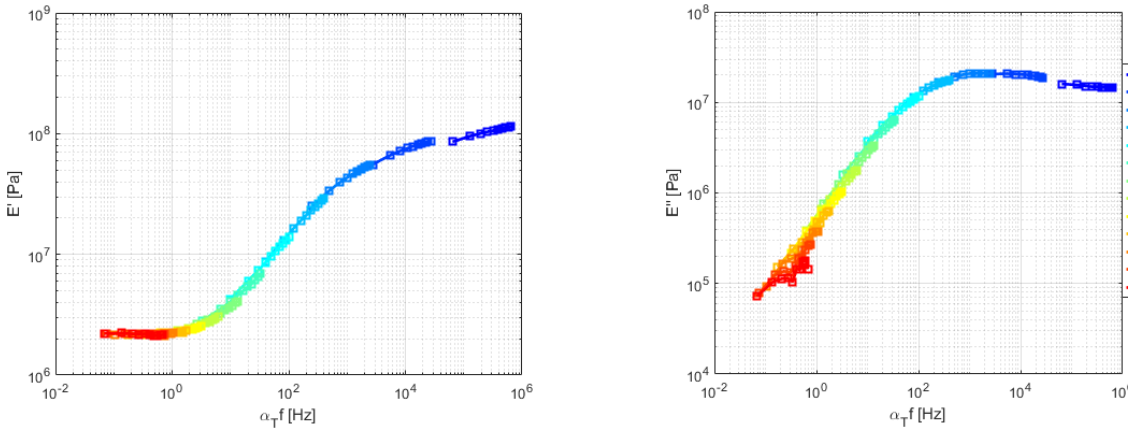

(a) (b)

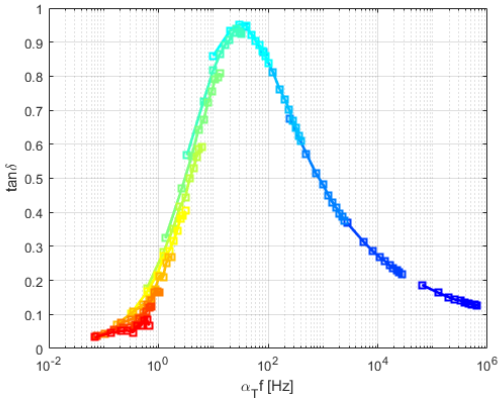

(c)

Figure 24– Master's curves of the PB 270i foam: storage modulus (a), loss modulus (b) and loss factor (c).

4.4 Synthesis of the foam characterization

The overall results of the microstructural and mechanical characterization, along with the parameters of the master curves for the foam system are summarized in the following table.

Material characterization after curing
Microstructure
Density : 0.272±0.007 g/cm^3
Bubble diameter : 264 ±102 µm
Quasi-static properties
E : 165 MPa
G : 61 MPa
ν : 0.35
Dynamic properties (WLF model)
T_{ref}: 145°C
C_1^{ref}: 4.811
C_2^{ref}: 44.639 K

Table 14: Summary of bulk foam characterization.

5. Conclusions

The present paper has dealt with the processing and characterization of an expandable epoxy foam in order to identify and model the most relevant phenomena involved with this material, from the processing conditions, to the microstructure and the static and dynamic mechanical characterizations. All the relevant parameters have been identified and will be of great interest for the future development of multi-functional structures based on this material as a core material for the sandwich structures. The approach used in the study is divided in two main areas: the processing analysis, the characterization and modelling of the PB270i foam with its hardener SD 2630. The processing conditions of the foam have been analysed using a classical kinetic and chemo-rheological approach. The DSC, rheology and foam expansion experiments have been conducted, analysed and modelled in agreement with the literature, using either physical or empirical models. The different models identified have then been used to plot the Temperature-Time-Transformation (TTT) diagrams of the foam. Several phenomena have been integrated in the diagrams as the foam gelification, the polymer gelification, the curing and the

vitrification of the final foam. The TTT diagrams have allowed analysing a specific curing cycle for the foam, showing in detail the evolution of the material Tg with the curing temperature. It has been shown that the model is in good agreement with the experimental results for low curing temperatures (20°C to 60°C), while it is less reliable when approaches the higher degree of conversion. This result has been attributed to the modelling assumption made, considering a unique model to represents the whole system over a wide range of temperatures. In addition, diffusion-controlled phenomena have been represented using a very simple approach. Nevertheless, the kinetic models integrated in the TTT diagram globally allow representing the transformation within the system with an acceptable degree of accuracy. In future works, diffusion-controlled kinetics in vitrification region and the temperature dependence of the expansion kinetics will be addressed in detail, in order to complete the constitutive behaviour of this system and improve the reliability for all the regions of the TTT diagram. The curing cycle selected has been used to produce several foam samples of various sizes and shapes that have been used to characterize the final bulk material. A microscopic analysis of the bubble size distribution has been performed using a statistical-imagery approach, followed by the analysis of the mechanical properties under quasi-static and dynamic conditions. The last part of the paper has focused on the validation of the Time-Temperature equivalence for the material, in order to identify the WLF model for the plotting of the Master curves of the foam and describe in detail its dynamic behaviour. The models obtained are in good agreement with the experimental data and constitute a good basis for further development of future MFS for aerospace applications. The PB270i expandable foam with its hardener SD 2630 represents a very interesting candidate to replace honeycomb core materials as Nomex®, given its good damping behaviour and the possibility to directly integrate any functional element within it.

Acknowledgements

This project received funding from the Clean Sky 2 Joint Undertaking (JU) under grant agreement No. 785462. The JU received support from the European Union´s Horizon 2020 (H2020) research and innovation program and the Clean Sky 2 JU members other than the Union.

The authors would like to thank Sicomin for the helpful discussions regarding their PB270i product.

References

[1] K. K. Sairajan, G. S. Aglietti, and K. M. Mani, "A review of multifunctional structure technology for aerospace applications," *Acta Astronautica*, vol. 120, Elsevier, pp. 30–42, 2016. doi: 10.1016/j.actaastro.2015.11.024.

[2] A. Treviso, B. van Genechten, D. Mundo, and M. Tournour, "Damping in composite materials: Properties and models," *Compos B Eng*, vol. 78, pp. 144–152, 2015.

[3] A. L. Araújo, P. Martins, C. M. Mota Soares, C. A. Mota Soares, and J. Herskovits, "Damping optimization of viscoelastic laminated sandwich composite structures," *Structural and Multidisciplinary Optimization*, vol. 39, p. 569, 2009.

[4] Sankaran, S, K. R. Sekhar, G. Raju, and M. N. J. Kumar, "Characterization of epoxy syntactic foams by dynamic mechanical analysis," *J Mater Sci*, vol. 41, pp. 4041–4046, 2006.

[5] R. L. Poveda, S. Achar, and N. Gupta, "Viscoelastic properties of carbon nanofiber reinforced multiscale syntactic foam," *Compos B Eng*, vol. 58, pp. 208–216, 2014.

[6] A. Asif, V. L. Rao, and K. N. Ninan, "Nanoclay reinforced thermoplastic toughened epoxy hybrid syntactic foam: Surface morphology, mechanical and thermo mechanical properties," *Materials Science and Engineering A*, vol. 527, pp. 6184–6192, 2010.

[7] V. C. Shunmugasamy, D. Pinisetty, and N. Gupta, "Viscoelastic properties of hollow glass particle filled vinyl ester matrix syntactic foams: effect of temperature and loading frequency," *Journal of Material Science*, vol. 48, pp. 1685–1701, 2013.

[8] D. Bonthu, H. S. Bharath, S. Gururaja, P. Prabhakar, and M. Doddamani, "3D printing of syntactic foam cored sandwich composite," *Composites Part C: Open Access*, vol. 3, p. 100068, 2020.

[9] H. S. Bharath, A. Sawardekar, S. Waddar, P. Jeyaraj, and M. Doddamani, "Mechanical behavior of 3D printed syntactic foam composites," *Composites structures*, vol. 254, p. 112832, 2020.

[10] A. Adessina, M. Hamdaoui, C. Xu, and E. M. Daya, "Damping properties of bi-dimensional sandwich structures with multi-layered frequency-dependent visco-elastic cores," *Compos Struct*, vol. 154, pp. 334–343, 2016.

[11] A. Shahdin, L. Mezeix, C. Bouvet, J. Morlier, and Y. Gourinat, "Fabrication and mechanical testing of glass fiber entangled sandwich beams: A comparison with honeycomb and foam sandwich beams," *Compos Struct*, vol. 90, pp. 404–412, 2009.

[12] S. C. Woody and S. T. Smith, "Damping of a thin-walled honeycomb structure using energy absorbing foam," *J Sound Vib*, vol. 291, pp. 491–502, 2006.

[13] M. Sauceau, J. Fages, A. Common, C. Nikitine, and E. Rodier, "New challenges in polymer foaming: A review of extrusion processes assisted by supercritical carbon dioxide," *Progress in Polymer Science (Oxford)*, vol. 36, no. 6, pp. 749–766, 2011, doi: 10.1016/j.progpolymsci.2010.12.004.

[14] B. V. Kichatov and A. M. Korshunov, "Nucleation of gas bubbles in extrusion foaming of high-pressure polyethylene," *Theoretical Foundations of Chemical Engineering*, vol. 39, no. 6, pp. 643–652, 2005, doi: 10.1007/s11236-005-0129-x.

[15] J. R. Robledo-Ortiz, C. Zepeda, C. Gomez, D. Rodrigue, and R. González-Núñez, "Non-isothermal decomposition kinetics of azodicarbonamide in high density polyethylene using a capillary rheometer," *Polym Test*, vol. 27, no. 6, pp. 730–735, 2008, doi: 10.1016/j.polymertesting.2008.05.004.

[16] A. Reglero-Ruiz *et al.*, "Polymer foaming with chemical blowing agents : Experiment and modeling To cite this version : HAL Id : hal-01102122 Polymer foaming with Chemical Blowing Agents : Experiment and modeling," *Polym Eng Sci*, pp. 2018–2029, 2015.

[17] R. Rao *et al.*, "A Kinetic Approach to Modeling the Manufacture of High Density Polyurethane Structural Foam: Foaming and Polymerization," 2015.

[18] B. Koohbor and A. Kidane, "Design optimization of continuously and discretely graded foam materials for efficient energy absorption," *Mater Des*, vol. 102, pp. 151–161, 2016, doi: 10.1016/j.matdes.2016.04.031.

[19] G. Wypych, *Handbook of Foaming and Blowing Agents*, First Edit., vol. 1. ChemTec Publishing, 2017.

[20] M. A. Shafi, J. G. Lee, and R. W. Flumerfelt, "Prediction of Cellular Structure in Free Expansion Polymer Foam Processing," *Polym Eng Sci*, vol. 36, no. 14, 1996.

[21] K. Joshi, J. G. Lee, M. A. Shafi, and R. W. Flumerfelt, "Prediction of cellular structure in free expansion of viscoelastic media," *J Appl Polym Sci*, vol. 67, no. 8, pp. 1353–1368, 1998, doi: 10.1002/(sici)1097-4628(19980222)67:8<1353::aid-app2>3.3.co;2-3.

[22] J. J. Feng and C. A. Bertelo, "Prediction of bubble growth and size distribution in polymer foaming based on a new heterogeneous nucleation model," *J Rheol (N Y N Y)*, vol. 48, no. 2, pp. 439–462, 2004, doi: 10.1122/1.1645518.

[23] A. Naber, C. Liu, and J. J. Feng, "The nucleation and growth of gas bubbles in a Newtonian fluid: an energetic variational phase field approach," vol. 466, no. 50390095, pp. 95–120, 2008, doi: 10.1090/conm/466/09118.

[24] Y. Kim, C. B. Park, P. Chen, and R. B. Thompson, "Origins of the failure of classical nucleation theory for nanocellular polymer foams," *Soft Matter*, vol. 7, no. 16, pp. 7351–7358, 2011, doi: 10.1039/c1sm05575e.

[25] K. Lee H., Neville, *Handbook of Epoxy Resin*. New York: McGraw-Hill, 1982.

[26] K. Kurek and A. Bledzki, "Mechanical behaviour of polyurethane- and epoxy foams and their glass fibre composites," *Mechanics of Composite Materials*, vol. 30, no. 2, pp. 155–161, 1994, Accessed: Nov. 04, 2022. [Online]. Available: https://doi.org/10.1007/BF00635839

[27] E. W. Burton, G.W., Carter, "Use of formed in place epoxy resins in aircraft composite structures," *Journal of Cellular Plastics*, vol. 5/6, pp. 140–145, 1971.

[28] M. L. Hobbs, "Modeling epoxy foams exposed to fire-like heat fluxes," *Polym Degrad Stab*, vol. 89, no. 2, pp. 353–372, 2005, doi: 10.1016/j.polymdegradstab.2005.01.021.

[29] C. S. Karthikeyan, S. Sankaran, and Kishore, "Elastic behaviour of plain and fibre-reinforced syntactic foams under compression," *Mater Lett*, vol. 58, no. 6, pp. 995–999, 2004, doi: 10.1016/j.matlet.2003.08.012.

[30] M. Mondy, L.A., Rao, R.R., Moffat, H., Adolf, D., Celina, "Structural Epoxy Foams," in *Epoxy Polymers - New Materials and Innovations*, Wiley-VCH., R. J. J. Pascault, J.P., Williams, Ed. 2010, pp. 303–324.

[31] P. M. Stefani, A. T. Barchi, J. Sabugal, and A. Vazquez, "Characterization of epoxy foams," *J Appl Polym Sci*, vol. 90, no. 11, pp. 2992–2996, 2003, doi: 10.1002/app.13006.

[32] S. H. Lee, H. Y. Song, D. G. Kim, S. W. Lim, E. Y. Park, and K. Hyun, "Investigation of foaming cell development for epoxy resin with blowing and curing agent by rheological properties," *Macromol Res*, vol. 25, no. 4, pp. 325–334, 2017, doi: 10.1007/s13233-017-5052-6.

[33] L. Wang, Y. Ji, and X. Peng, "A new two-step process to prepare microcellular epoxy foams based on kinetic analysis," *J Mater Sci*, vol. 53, no. 2, pp. 1540–1555, 2018, doi: 10.1007/s10853-017-1583-7.

[34] X. Wu *et al.*, "Recent developments on epoxy-based syntactic foams for deep sea exploration," *J Mater Sci*, vol. 56, no. 3, pp. 2037–2076, 2021, doi: 10.1007/s10853-020-05420-w.

[35] E. Finter, J., Jendoubi, “Heat curable epoxy resin composition with water as foaming agent,” US9475904B2, 2010

[36] W. R. Wismer, M., Hydro, “Method of foaming an admixture of epoxy resin, a chlorofluorocarbon, and a curing catalist,” U.S. Patent No. 3,051,665

[37] F. Quadrini and E. A. Squeo, “Solid-state foaming of epoxy resin,” *Journal of Cellular Plastics*, vol. 44, no. 2, pp. 161–173, 2008, doi: 10.1177/0021955X07082486.

[38] A. Moser, “Expandierende epoxide-laminiersysteme,” in *Conference VERBUDWERK*, 1990, pp. 5.1-5.20.

[39] A. A. Abraham, R. Chauhan, A. K. Srivastava, M. Katiyar, and D. N. Tripathi, “Mechanical, Thermal and Electrical Properties of Epoxy Foam,” *Journal of Polymer Materials*, vol. 28, pp. 267–274, Apr. 2011.

[40] H. H. Chen, “Foamed Resin Obtained by the Reaction of Polyepoxide, a Trialboroxine, and an Amine,” No. 3,025,249

[41] T. Matsuda, “Japanese Patent No. 50-6665,” 1975

[42] K. Takiguchi, O., Ishikawa, D., Sugimoto, M., Taniguchi, T., Koyama, “Effect of Rheological Behavior of Epoxy during Precuring on Foaming,” *J Appl Polym Sci*, vol. 110, no. 2, pp. 657–662, 2008.

[43] Sicomin, “PB270i, PB 370i & PB 570 i Fireproof autoextinuishing foaming epoxy systems,” 2016. http://sicomin.com/datasheets/product-pdf205.pdf

[44] Sicomin, “SR 1660 Heat resistant epoxy systems,” 2016. http://sicomin.com/datasheets/product-pdf41.pdf

[45] A. T. Di Benedetto, “Prediction of the glass transition temperature of polymers: a model based on the principle of corresponding states,” *Journal of Polymer Science: Part B*, vol. 25, pp. 1949–1969, 1987.

[46] J. K. Gillham, “Torsional Braid Analysis (TBA) of polymers,” in *Development in Polymer Characterization-3*, J.V. Dawju., A. Science, Ed. 1982, p. 159.

[47] M. T. Aronhime and J. K. Gillham, “Time-Temperature-Transformation (Ttt) Cure Diagram of Thermosetting Polymeric Systems.,” *Advances in Polymer Science*, vol. 78, pp. 83–113, 1986, doi: 10.1007/bfb0035358.

[48] M. Ivankovic, L. Incarnato, J. M. Kenny, and L. Nicolais, “Curing kinetics and chemo-rheology of epoxy/anhydride system,” *J Appl Polym Sci*, vol. 90, pp. 3012–3019, 2003.

[49] F. X. Perrin, T. M. H. Nguyen, and J. L. Vernet, “Chemico-diffusion kinetics and TTT cure diagrams of DGEBA–DGEBF/amine resins cured with phenol catalysts,” *Eur Polym J*, vol. 43, no. 12, pp. 5107–5120, 2007, doi: 10.1016/j.eurpolymj.2007.09.020.

[50] N. Rabearison, Ch. Jochum, and J. C. Grandidier, “A cure kinetics, diffusion controlled and temperature dependent, identification of the Araldite LY556 epoxy,” *J Mater Sci*, vol. 46, no. 3, pp. 787–796, 2010.

[51] P. I. Karkanas and I. K. Partridge, “Cure Modeling and Monitoring of Epoxy/Amine Resin Systems. I. Cure Kinetics Modeling,” *J Appl Polym Sci*, vol. 77, pp. 1419–1431, 2000.

[52] P. I. Karkanas and I. K. Partridge, “Cure Modeling and Monitoring of Epoxy/Amine Resin Systems. II. Network Formation and Chemoviscosity Modeling,” *J Appl Polym Sci*, vol. 77, pp. 2178–2188, 2000.

[53] R. D’Elia, G. Dusserre, S. Del Confetto, N. Eberling-Fux, C. Descamps, and T. Cutard, “Cure kinetics of a polysilazane system: Experimental characterization and numerical modelling,” *Eur Polym J*, vol. 76, 2016, doi: 10.1016/j.eurpolymj.2016.01.025.

[54] R. D’Elia, G. Dusserre, S. del Confetto, N. Eberling-Fux, C. Descamps, and T. Cutard, “Effect of dicumyl peroxide concentration on the polymerization kinetics of a polysilazane system,” *Polym Eng Sci*, 2017, doi: 10.1002/pen.24638.

[55] H. L. Friedman, “Kinetics of Thermal Degradation of Char-Forming Plastics from Thermogravimetry. Application to a Phenolic Plastic,” *Journal of Polymer Science: Part C*, no. 6, pp. 183–195, 1964.

[56] S. V. Vyazovkin and A. I. Lesnikovich, “Estimation of the pre-exponential factor in the isoconversional calculation of effective kinetic parameters,” *Thermochim Acta*, vol. 128, no. C, pp. 297–300, 1988, doi: 10.1016/0040-6031(88)85372-3.

[57] S. Vyazovkin and N. Sbirrazzuoli, “Mechanism and kinetics of epoxy-amine cure studied by differential scanning calorimetry,” *Macromolecules*, vol. 29, no. 6, pp. 1867–1873, 1996, doi: 10.1021/ma951162w.

[58] S. Vyazovkin and N. Sbirrazzuoli, “Isoconversional kinetic analysis of thermally stimulated processes in polymers,” *Macromol Rapid Commun*, vol. 27, no. 18, pp. 1515–1532, 2006, doi: 10.1002/marc.200600404.

[59] C. Schick, *Handbook of Thermal Analysis and Calorimetry*, vol. 5, no. C. 2008. doi: 10.1016/S1573-4374(13)60004-7.

[60] M. R. Kamal and S. Sourour, “Kinetics and Thermal Characterization of Thermoset Cure,” *Polym Eng Sci*, vol. 13, no. 1, pp. 59–64, 1973.

[61] C. Paris, “Étude et modélisation de la polymérisation dynamique de composites à matrice thermodurcissable,” 2011.

[62] J. A. Nelder and R. Mead, “A simplex method for function minimization,” *Computer Journal*, vol. 7, no. 4, pp. 308–313, 1965.

[63] J. C. Lagarias, J. A. Reeds, M. H. Wright, and P. E. Wright, “Convergence Properties of the Nelder-Mead Simplex Method in Low Dimensions,” *SIAM Journal of Optimization*, vol. 9, no. 1, pp. 112–147, 1998.

[64] M. Harsch and J. Herzog, F. Karger-Kocsis, “Cure-induced normal force development in unfilled and filled epoxy resins,” *J Compos Mater*, vol. 42, pp. 2299–2309, 2008.

[65] P. J. Shah, D.U. and Schubel, “Evaluation of cure shrinkage measurement techniques for thermosetting resins,” *Polym Test*, vol. 29, pp. 629–639, 2010.

[66] D. Harran and A. Laudouard, “Caractérisation de la gélification d’une résine thermodurcissable par méthode rhéologique,” *Rheol Acta*, vol. 24, pp. 596–602, 1985.

[67] M. Hayaty, M., Beheshty, M. H., Esfandeh, “A new approach for determination of gel time of a glass/epoxy prepreg,” *J Appl Polym Sci*, vol. 120, no. 3, pp. 1483–1489, 2010.

[68] R. H. S.R. Raghavan, L.A. Chan, C. McDowell, S.A. Khan and S. White, “Rheological study of crosslinking and gelation in chlorobutyl elastomer systems,” *Polymer (Guildf)*, vol. 37, pp. 5869–5875, 1996.

[69] J. A. Bouayad, D., Bikard, J., Agassant, “Compressible flow in a plate/plate rheometer: application to the experimental determination of reactive expansion’s models parameters for polyurethane foam,” *International Journal of Material Forming*, vol. 2, no. 4, pp. 243–260, 2009.

[70] C. W. Artavia, L.D., Macosko, “Foam kinetics,” in *Proceedings of the SPI 33rd Annual Technical/Marketing Conference*, 1990, pp. 55–561.

[71] A. J. Elwell, M.J., Ryan, “In-situ studies of structure development during the reactive processing of model flexible polyurethane foam systems using FT-IR spectroscopy, synchrotron SAXS, and rheology,” *Macromolecules*, vol. 29, pp. 2960–2968, 1996.

[72] N. John, R., Trachil, E.B., Neelakantan, N.R., Subramanian, “A viscometric approach to the study of the kinetics of polyurethane reactions,” *Polym Plast Technol Eng*, vol. 30, pp. 545–557, 1991.

[73] F. Jurine, S., Cox, S., Graner, “Dry three-dimensional bubbles: growth rate, scaling state and correlations,” *Colloid Surface A physicochemical Engineering Aspects*, vol. 263, no. 1–3, pp. 18–26, 2005.

[74] C. W. Mora, E., Artavia, L.D., Macosko, “Modulus development during reactive urethane foaming,” *J Rheol (N Y N Y)*, vol. 35, no. 5, pp. 921–940, 1991.

[75] F. Thomas, G.L., de Almeida, R.M.C., Graner, “Coarsening of three-dimensional grains in crystals, or bubbles in dry foams, tends towards a universal, statistically scale-invariant regime,” *Phys Rev E Stat Nonlin Soft Matter Phys*, vol. 74, no. 2 Part 1, 2006.

[76] Ira. N. Levine, *Physical Chemistry*. University of Brooklyn, 1978.

[77] T. M. H. Nguyen, “Systèmes epoxy-amine incluant un catalyseur externe phénolique : cinétique de réticulation -vieillissement hydrolytique,” Université du Sud-Toulon-Var, 2007.

[78] TA, “Thermal solutions - Characterization of Epoxy Reinforced Glass by DSC and DMA.”

[79] H. Leaderman, “Textile materials and time factor,” *Textile Research Journal*, 1941.

[80] C. D. Han and J. K. Kim, “On the use of time-temperature superposition in multicomponent/multiphase polymer systems,” *Polymer (Guildf)*, vol. 34, no. 12, pp. 2533–2539, 1993.

[81] M. Van Gurp and J. Palmen, “Time-temperature superposition for polymeric blends,” *Rheology bulletin*, 1998.

[82] M. L. Williams, R. F. Landel, and J. D. Ferry, “The Temperature Dependence of Relaxation Mechanisms in Amorphous Polymers and Other Glass-forming Liquids,” *Journal of American Chemical Society*, vol. 77, no. 14, pp. 3701–3707, 1955.